



**HAL**  
open science

# Paleolakes, paleofloods, and depressions in Aurorae and Ophir plana, Mars: Connectivity of surface and subsurface hydrological systems

Goro Komatsu, Gaetano Di Achille, Ciprian Popa, Stefano Di Lorenzo,  
Angelo Pio Rossi, Jose Alexis Palmero Rodriguez

► **To cite this version:**

Goro Komatsu, Gaetano Di Achille, Ciprian Popa, Stefano Di Lorenzo, Angelo Pio Rossi, et al.. Paleolakes, paleofloods, and depressions in Aurorae and Ophir plana, Mars: Connectivity of surface and subsurface hydrological systems. *Icarus*, 2009, 201 (2), pp.474. 10.1016/j.icarus.2009.01.010 . hal-00533498

**HAL Id: hal-00533498**

**<https://hal.science/hal-00533498>**

Submitted on 7 Nov 2010

**HAL** is a multi-disciplinary open access archive for the deposit and dissemination of scientific research documents, whether they are published or not. The documents may come from teaching and research institutions in France or abroad, or from public or private research centers.

L'archive ouverte pluridisciplinaire **HAL**, est destinée au dépôt et à la diffusion de documents scientifiques de niveau recherche, publiés ou non, émanant des établissements d'enseignement et de recherche français ou étrangers, des laboratoires publics ou privés.

## Accepted Manuscript

Paleolakes, paleofloods, and depressions in Aurorae and Ophir plana,  
Mars: Connectivity of surface and subsurface hydrological systems

Goro Komatsu, Gaetano Di Achille, Ciprian Popa,  
Stefano Di Lorenzo, Angelo Pio Rossi,  
Jose Alexis Palmero Rodriguez

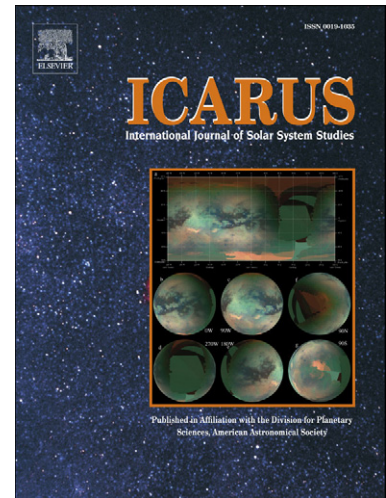
PII: S0019-1035(09)00032-3  
DOI: [10.1016/j.icarus.2009.01.010](https://doi.org/10.1016/j.icarus.2009.01.010)  
Reference: YICAR 8892

To appear in: *Icarus*

Received date: 1 October 2008  
Revised date: 23 January 2009  
Accepted date: 23 January 2009

Please cite this article as: G. Komatsu, G. Di Achille, C. Popa, S. Di Lorenzo, A.P. Rossi,  
J.A.P. Rodriguez, Paleolakes, paleofloods, and depressions in Aurorae and Ophir plana, Mars:  
Connectivity of surface and subsurface hydrological systems, *Icarus* (2009), doi:  
[10.1016/j.icarus.2009.01.010](https://doi.org/10.1016/j.icarus.2009.01.010)

This is a PDF file of an unedited manuscript that has been accepted for publication. As a service to our customers we are providing this early version of the manuscript. The manuscript will undergo copyediting, typesetting, and review of the resulting proof before it is published in its final form. Please note that during the production process errors may be discovered which could affect the content, and all legal disclaimers that apply to the journal pertain.



1 **Paleolakes, paleofloods, and depressions**  
2 **in Aurorae and Ophir plana, Mars:**  
3 **Connectivity of surface and subsurface hydrological systems**  
4

5 Goro Komatsu<sup>1</sup>, Gaetano Di Achille<sup>1,2</sup>, Ciprian Popa<sup>3,4</sup>,  
6 Stefano Di Lorenzo<sup>1</sup>, Angelo Pio Rossi<sup>5</sup>, Jose Alexis Palmero Rodriguez<sup>6</sup>  
7  
8

9 <sup>1</sup>International Research School of Planetary Sciences  
10 Università d'Annunzio, Viale Pindaro 42, 65127 Pescara  
11 Italy  
12

13 <sup>2</sup>Now at: Laboratory for Atmospheric and Space Physics  
14 University of Colorado, Boulder, Colorado 80309  
15 USA  
16

17 <sup>3</sup>Osservatorio Astronomico di Capodimonte  
18 Salita Moiariello 16, 80131 Napoli  
19 Italy  
20

21 <sup>4</sup>Department of Geology  
22 University "Al. I. Cuza"  
23 Iasi, Bulevardul Carol I, Nr.11, 700506  
24 Romania  
25

26 <sup>5</sup>International Space Science Institute  
27 Hallerstrasse 6, CH-3012 Bern, CH  
28 Switzerland  
29

30 <sup>6</sup>Planetary Science Institute  
31 Tucson, Arizona 85719  
32 USA  
33

34 48 pages of text, 1 table, and figure captions  
35 16 figures  
36

37  
38  
39  
40  
41  
42  
43  
44  
45  
46  
47  
48  
49  
50  
51  
52  
53  
54  
55

Proposed running head:  
Paleolakes and paleofloods in Aurorae and Ophir plana

Corresponding author: Goro Komatsu

International Research School of Planetary Sciences  
Università d'Annunzio, Viale Pindaro 42  
65127 Pescara  
Italy

Tel.: +39-085-453-7507; fax: +39-085-453-7545.

*E-mail address:* goro@irsps.unich.it (G. Komatsu).

56

**Abstract**

57

58 The plains of Aurorae and Ophir in the equatorial region of Mars display extensive  
59 geomorphic evidence indicative of paleo-hydrological processes linking surface and  
60 subsurface. Elaver Vallis in Aurorae Planum south of Ganges Chasma is an outflow  
61 channel system >180 km long, and here inferred to have formed by cataclysmic  
62 spillover flooding from a paleolake(s) contained within the Morella crater basin.  
63 Ganges Cavus is an enormous 5-km-deep depression of probable collapse origin located  
64 within the Morella basin. The fluid responsible for the infilling of the Morella basin  
65 may have emerged at least partially through Ganges Cavus or its incipient depression.  
66 The fluid may have been supplied also from small-scale springs within the basin. It is  
67 reasonable to assume that water, sometimes sediment-laden and/or mixed with gases,  
68 was the responsible fluid for these phenomena. Similar paleo-hydrological processes  
69 are inferred also in Ophir Planum. Water emergence may have occurred as  
70 consequences of ground ice melting or breaching of cryosphere to release water from  
71 the underlying hydrosphere. Dike intrusion is considered to be an important cause of  
72 formation for the cavi and smaller depressions in Aurorae and Ophir plana, explaining  
73 also melting of ground ice or breaching of cryosphere. Alternatively, the depressions

74 and crater basins may have been filled by regional groundwater table rising during the  
75 period(s) when cryosphere was absent or considerably thin. In both cases, the large  
76 quantities of water necessary for explaining the paleo-hydrological processes in Aurorae  
77 and Ophir plana may have been derived through crustal migration from the crust of  
78 higher plains in western Ophir Planum where water existed in confined aquifers or was  
79 produced by melting of ground ice due to magmatic heating or climatic shift, or from a  
80 paleolake in Candor Chasma further west.

81

82 **Keywords:** Mars, Surface; Geological Processes; Mineralogy

83 **1. Introduction**

84

85 Water on Mars is a subject of paramount importance. Among various water-related  
86 processes on the planet, there are long histories of studies on paleo-crater lakes (e.g.,  
87 Cabrol and Grin, 1999; Ori et al., 2000; Malin and Edgett, 2003; Pondrelli et al., 2005;  
88 Di Achille et al., 2006) and cataclysmic flood channels (e.g., Baker and Milton, 1974;  
89 Baker, 1978; Komatsu and Baker, 1997; Burr et al., 2002). The Valles  
90 Marineris-chaotic terrain transition zone on Mars (**Fig. 1**) is characterized by  
91 morphologic and morphometric characteristics that are commonly interpreted to be  
92 indicative of interactions between hydrologic and tectonomagmatic activities (e.g.,  
93 Rotto and Tanaka, 1995; Mège and Masson, 1996c; Dohm et al., 2002; Chapman and  
94 Tanaka, 2002; Greeley et al., 2003; Komatsu et al., 2004; Rodriguez et al., 2006).  
95 Excellent examples of paleo-crater lakes, outflow channels, and their associated  
96 collapse features are present in this zone, providing an opportunity for assessing their  
97 inter-relationships in detail. We use the term “depression” for the collapse features in  
98 this paper in order to distinguish them from impact crater basins. And the data sets  
99 acquired by the Mars Global Surveyor and Mars Odyssey missions have already shed  
100 new light on the lacustrine-fluvial history and possible recharging mechanisms (e.g.,

101 Coleman et al., 2003; Harrison and Grimm, 2004; Russell and Head, 2007; Coleman et  
102 al., 2007; Coleman and Dinwiddie, 2007).

103 Coleman et al. (2007) conducted the first comprehensive study of Aurorae and Ophir  
104 plana, the plains near Ganges Chasma (**Figs. 1, 2**) in the Valles Marineris-chaotic terrain  
105 transition zone, described an outflow channel called Allegheny Vallis, and concluded  
106 that the floodwater emerged from the subsurface through a depression called Ophir  
107 Cavus. They also concluded that an ice-covered paleolake in Candor Chasma to the  
108 west of Aurorae and Ophir plana may have been the original source of the water that  
109 eventually emerged in Ophir Cavus.

110 In this paper, we present results of a combined morphological, topographical and  
111 spectroscopic analysis of Aurorae and Ophir plana utilizing newly available  
112 remote-sensing data from the Mars Express and Mars Reconnaissance Orbiter missions.  
113 In particular, we investigated evidence of various paleolakes formed by groundwater  
114 emergence and their relationship with outflow events. We also discuss about possible  
115 mechanisms of subsurface water migration and its emergence in the region.

116

## 117 **2. Method**

118

119 An integrated analysis utilizing a multi-spatial-resolution, multi-spectral planetary  
120 data set allows simultaneous interpretations of landforms in regional to local contexts.  
121 In this study, we investigated areas in Aurorae and Ophir plana using Viking imagery,  
122 Mars Orbiter Laser Altimeter (MOLA) Digital Elevation Models (DEMs), wide and  
123 narrow angle Mars Orbiter Camera (MOC) images, Thermal Emission Imaging System  
124 (THEMIS) visible (VIS) and infrared (IR, both daytime and nighttime) images, High  
125 Resolution Stereo Camera (HRSC) images, and High Resolution Imaging Science  
126 Experiment (HiRISE) images. The remote sensing images were radiometrically and  
127 geometrically calibrated with the United States Geological Survey - Integrated Software  
128 for Imagers and Spectrometers (ISIS) software system.

129 Topography and image data were projected using the IAU 2000 reference ellipsoid  
130 for Mars (Seidelmann et al, 2002). Topographic and imagery data were map-projected  
131 and integrated into a GIS system. The projection used for geological and  
132 geomorphological mapping is Mercator, with both latitude and longitude centered at  
133 zero. Area or length measurements were performed with equal-area and equi-distant  
134 projections respectively. MOLA PEDR profiles (Smith et al., 1999) were interpolated  
135 with the Generic Mapping Tools (Wessel and Smith, 1998) at a spatial resolution of  
136  $1/128^\circ$  per pixel. Absolute height values were referred to the gridded PEDR.

137 Impact crater counting was conducted on THEMIS daytime and nighttime infrared  
138 images (at 100 m/pixel). The minimum crater diameter taken into account for the  
139 crater counting is 1 km. Calibration to absolute age was based on Hartmann (1999),  
140 Hartmann and Neukum (2001), and Ivanov (2001). The time-stratigraphic assignment  
141 was based on Tanaka et al. (1992).

142 The Observatoire pour la Minéralogie, l'Eau, les Glaces et l'Activité (OMEGA) is a  
143 visible - near infrared (VIS-NIR) image spectrometer that covers the spectral range of  
144 0.38–5.1  $\mu\text{m}$ , subdivided into three channels. The data along with the processing  
145 software are available online at the ESA Planetary Science Archive. The OMEGA  
146 data were processed using the "readomega" software version 4 released through the  
147 PDS node, and a custom IDL procedure was written to remove the atmosphere using a  
148 scaled ratio spectrum of Olympus Mons base and top (summit), considering a constant  
149 IR response (the same composition) over the flanks of Olympus Mons. Assuming this  
150 as the average atmosphere contribution, each spectrum in OMEGA images is divided by  
151 the "Olympus Mons" spectrum scaled for the main  $\text{CO}_2$  absorption at 2.0  $\mu\text{m}$ . The  
152 OMEGA analysis was conducted in the region of Aurorae Planum where the data  
153 coverage of public release is reasonable. Several OMEGA orbits cover the area of  
154 interest and were analyzed in order to derive maps from spectral signatures detectable in

155 the spectral range of OMEGA C (court) channel: pyroxene, olivine and hydrated  
156 minerals: 0394\_2, 0894\_2, 0905\_6, 0916\_6, 0938\_6, 0971\_5, 1004\_6, 1015\_6, 1264\_1,  
157 1297\_1, 1341\_2, 1513\_5, 1590\_5. The above orbits either cover the area of interest,  
158 either overlap orbits of interest in order to compare a certain spectral feature observed  
159 on the ground to isolate it from possible interferences due to water ice clouds or  
160 atmospheric residuals from the atmospheric correction itself.

161 The OMEGA C channel data corrected with the method described above were  
162 successfully used to unambiguously map mafic mineral contents of Martian surface in  
163 terms of high and low calcium pyroxenes as well as Mg and Fe end members of olivine  
164 solid solution (forsterite and fayalite) (Mustard et al., 2005; Poulet et al., 2007). Maps  
165 for the minerals of interest are derived using the spectral parameters defined by Poulet  
166 et al. (2007). These spectral parameters represent the band depths at 1  $\mu\text{m}$  for Mg-rich  
167 olivine (forsterite), and Fe-rich olivine (fayalite) with grain size  $>1$  mm, 2  $\mu\text{m}$  band for  
168 pyroxenes (low and high calcium pyroxene). See Poulet et al. (2007) for a detailed  
169 description on spectral parameters. In order to avoid “false positive” detection of  
170 minerals, we chose thresholds for detection limits (lower limits) as follows: pyroxene  
171 0.01, forsterite 1.04, fayalite 1.02 (Poulet et al., 2007).

172 The detailed OMEGA analysis result is presented for the orbit 0394\_2 that covers

173 western two-third of the Morella basin. The orbit was chosen because it has a  
174 relatively high spatial resolution (~1.1 km), and the detected spectral units in this data  
175 set are well correlated with albedo features or geomorphologically distinctive units on  
176 the surface, and most importantly it has low 2.0  $\mu\text{m}$  water ice clouds absorption band.

177

### 178 **3. Geomorphological units**

179

180 Ganges, Eos-Capri chasmata and their surroundings (**Fig. 1**) are characterized by  
181 major geomorphological units including canyons, chaotic terrains, plains, interior  
182 layered deposits, craters, and channels. Many north-south-trending wrinkle ridges  
183 (~10 km in width) cross the plains. We measured the cumulative crater population  
184 density of the plains unit around Ganges Chasma (**Fig. 3**). Assuming that the counted  
185 craters are of impact origin, the result indicates that the overall plains surfaces range  
186 from Late Noachian to Early Hesperian in age. This is consistent with the Noachian to  
187 Hesperian ages derived by Scott and Tanaka (1986).

188 Aurorae and Ophir plana are covered with many circular basins that are probably  
189 impact craters of various sizes and degradation states (**Fig. 2**). An outflow channel  
190 system called Elaver Vallis is observed in Aurorae Planum south of Ganges Chasma,

191 and it is connected with the Morella basin and terminates at the southern edge of  
192 Ganges Chasma. Another outflow channel system called Allegheny Vallis occurs in  
193 Ophir Planum west of Ganges Chasma, and it terminates at the western edge of Ganges  
194 Chasma.

195

#### 196 **4. Elaver Vallis and Morella paleolake**

197

##### 198 *4.1. Elaver Vallis, an outflow channel system*

199

200 *Observations:* Elaver Vallis is a >180-km-long, 70-km-wide channel system emanating  
201 from Morella, a crater basin 70–80 km in diameter (**Figs. 2, 4, 5, 7, 8**). It is  
202 characterized by an anastomosing pattern in its middle reach, and its floors are  
203 longitudinally grooved. The lowermost reach of the channel system is a deep  
204 V-shaped canyon with a theater-like head, which is distinctively different from the  
205 anastomosing middle reach. Sediments accumulated on the bottom of Ganges Chasma  
206 below the mouth of the V-shaped canyon, forming a large fan complex (**Fig. 4**). This  
207 large Elaver fan complex is adjacent to a series of smaller fans to both east and west  
208 directions along the canyon walls. All these fans have cone shapes typical of alluvial

209 fans, and their coalescence classifies them as bajadas. The Elaver fan complex has an  
210 erosional margin that cuts an adjacent smaller fan to the west, indicating its later  
211 formation at least at its last stage of development (**Fig. 4**).

212 A cross-cutting relationship of grooves is observed (**Fig. 6a**), implying progressive  
213 incision in the topographically lower reach during a single event or multiple events. A  
214 portion of plains to the east of the Elaver Vallis mouth is grooved in a manner similar to  
215 the floors of Elaver Vallis (**Fig. 6b**). The east-west orientation of the grooves and their  
216 elevations similar to those of the grooved lower reach of Elaver Vallis (**Fig. 5**) imply a  
217 genetic link between the two grooved areas. Patches of chaotic terrain are distributed  
218 on channel floors in the anastomosing middle reach (**Figs. 4, 6c**).

219 *Interpretations:* The large dimensions, the anastomosing pattern and longitudinal  
220 grooves of probable erosional origin are consistent with the formation of Elaver Vallis  
221 by flooding of a cataclysmic nature, similar to the floods that are considered to have  
222 formed outflow channels in the circum-Chryse region and elsewhere (e.g., Baker and  
223 Milton, 1974; Baker, 1978, 1982; Komatsu and Baker, 1997). Elaver Vallis is  
224 interpreted to be an outflow channel system formed by spillover from the Morella basin:  
225 a paleolake formed within the Morella basin and eventually reached the spillover level,  
226 breaching the crater rim and flooding Aurorae Planum to the east, and formed Elaver

227 Vallis. This type of spillover flooding has been hypothesized for terrestrial  
228 cataclysmic floods including the Bonneville flooding in western U.S.A. (O'Connor,  
229 1993) and the Manych flooding from paleo-Caspian Sea (Komatsu and Baker, 2007),  
230 and for the Ma'adim Vallis flooding from the Eridania basin on Mars (Irwin et al., 2002).  
231 Although non-aqueous, for example, CO<sub>2</sub> outburst hypotheses (e.g., Hoffman, 2000)  
232 may not be totally ruled out, it is generally believed that CO<sub>2</sub> flow, liquid and/or gas,  
233 lacks the capacity for producing the diverse range of morphology observed at Elaver  
234 Vallis (e.g., Coleman, 2003). The volcanic hypothesis proposed by Leverington  
235 (2004) for outflow channels is not totally ruled out, but no clear lava flow morphology  
236 (e.g., rough lava surfaces, flow margins) is observed along the Elaver Vallis reaches  
237 even with high-resolution images.

238 It is difficult to clearly determine the frequency and magnitude of the Elaver Vallis  
239 flooding from the available information alone. Almost the entire plains east of the  
240 Morella basin is below an elevation level of 1800 m, and the majority of channel floors  
241 are below 1600 m (**Fig. 5b**). For the single-flood hypothesis, a wide sheet flood is  
242 expected to occur at the early phase of cataclysmic flooding. And the flood flow may  
243 have expanded beyond the northern bank of Elaver Vallis. However, we do not see  
244 clear erosional flood morphologies such as grooves on the plains materials north of

245 Elaver Vallis. This indicates that the sheet flood neither passed over nor left erosional  
246 features on these materials perhaps because it effectively and rapidly excavated an  
247 incipient channel. As the flooding progressed, deep incision took place and the flood  
248 flow was more confined. Alternatively, the high degree of floodwater dissipation led  
249 to extensive sedimentary deposition during the early stages of outflow channel activity.  
250 The central channel of Elaver Vallis is below 1500 m (**Fig. 5b**). Thus the observation  
251 of the cross-cutting relationship of grooves in **Fig. 6a** is consistent with the deep  
252 incision in the central channel.

253 For the multiple-flood hypothesis, earlier floods may have eroded the  
254 topographically higher reaches, then later floods incised lower reaches. As discussed  
255 later, the spillway of the Morella basin rim appears to have been progressively cut low  
256 by the flood action. If this was the case, earlier floods could have taken advantage of  
257 higher potential energy from higher elevations and also larger volumes of the lakes, thus  
258 discharges for earlier floods should have been larger than those of later floods. A more  
259 precise assessment of flood discharge and inundation would require usage of numerical  
260 computer simulation programs such as the one employed by Miyamoto et al. (2006,  
261 2007).

262 The MOLA-derived longitudinal profiles and cross-sectional profiles (**Fig. 7**)

263 provide additional information on the origins of Elaver Vallis and its source area. We  
264 calculated a discharge rate range for the Elaver Vallis flooding using Manning's  
265 equation modified for Mars (e.g., Komar, 1979). We assumed that post-flood  
266 degradation and sedimentation of the channel are negligible although later flow events  
267 from patches of chaotic terrain may have contributed to further incision of the channel  
268 floors. In the lower middle reach of Elaver Vallis, the average slope is about 0.003,  
269 which we used to approximate the energy slope. We use the average flow depth in  
270 place of the hydraulic radius on the assumption that the flow width was significantly  
271 wider than the depth. The average flow depth range used in the calculation is 30–400  
272 m. The 30-m floodwater depth is a realistic lower limit for Martian outflow channels  
273 based on expected rates of evaporation and freezing (Wilson et al., 2004). For the  
274 upper flow depth, a value of 400 m was derived from the deepest depth of the lower  
275 middle reach. This is based on a bankfull discharge assumption for simplicity,  
276 although this assumption may not be applicable for outflow channels on Mars as  
277 suggested by others (e.g., Williams et al., 2000; Wilson et al., 2004; Coleman, 2005).  
278 We note that highwater marks that can be used to constrain the maximum possible  
279 discharge rate are difficult to be determined in Elaver Vallis, and the bankfull discharge  
280 assumption is helpful in the comparison with previous estimates that were often

281 conducted with the same assumption. The Manning coefficient (friction factor) was  
282 assumed to be 0.04–0.06, bracketing the number 0.0545 recommended by Wilson et al.  
283 (2004). The calculated discharge rate is in the range of  $10^6$ – $10^8$  m<sup>3</sup> s<sup>-1</sup>.

284 These values are at least an order of magnitude smaller than the values estimated for  
285 the largest circum-Chryse outflow channels (e.g., Robinson and Tanaka, 1990).  
286 Nevertheless, the discharge rates could have been equivalent or exceeded those  
287 estimated for the greatest terrestrial cataclysmic flood events ( $10^6$ – $10^7$  m<sup>3</sup> s<sup>-1</sup>) such as  
288 the Glacial Lake Missoula flooding in the northwestern United States, or the Altai and  
289 Yenisei flooding in Central Asia, which resulted from ice-dam failure(s) (e.g., O'Connor  
290 and Baker, 1992; Baker et al. 1993; Komatsu et al., 2009). Therefore it is an indication  
291 of cataclysmic nature of the spillover from the Morella basin. The discharge rate range  
292 of  $10^6$ – $10^8$  m<sup>3</sup> s<sup>-1</sup> is also consistent with the maximum volume of water available for  
293 flooding in the hypothesized Morella paleolake (2396 km<sup>3</sup>; see section 4.2.).

294 The lowermost reach of Elaver Vallis is characterized by a much steeper gradient  
295 (~0.13) but the flows during the presumed headward recession probably remained at  
296 relatively low discharge rates if the flows ever existed as surface runoff. We  
297 hypothesize the deep V-shaped canyon with a theater-like head to have formed after the  
298 major flooding by headward scarp recession along a pre-existing channel floor by

299 processes such as groundwater sapping or debris flows. The V-shaped canyon and the  
300 Elaver fan complex may have formed during the late-stage epoch of intense fluvial  
301 activity (latest Noachian to early to mid-Hesperian), which was discussed by Howard et  
302 al. (2005).

303 Grooves are observed on a portion of plains not directly connected with Elaver Vallis  
304 (**Fig. 6b**). The responsible flood for the grooves was likely the same as the one from  
305 the Morella basin, implying that the canyon geometry in this area during the flooding  
306 was not exactly the same as today. Backwasting or downfaulting of canyon walls  
307 probably continued after the flooding, and these are likely the causes of the canyon wall  
308 modification.

309 The type of chaotic terrains identified in the middle reach of Elaver Vallis (**Figs. 4,**  
310 **6c**) is also known in other areas including at Ravi Vallis (Coleman, 2005) and at a  
311 tributary of Ares Vallis (Rodriguez et al., 2005b). Their formation may have been  
312 related to flood excavation down to the cryosphere/hydrosphere contact (Coleman,  
313 2005) or destabilized icy deposits along the channel (Rodriguez et al., 2005b).

314

315 *4.2. Morella paleolake*

316

317 *Observations:* The Morella basin exhibits diverse features that indicate its complex  
318 history (**Fig. 8**). The basin rim in the east is open as a spillway for Elaver Vallis, and  
319 grooves are observed nearby (**Fig. 9a**). A discontinuous chain of degraded terraces is  
320 observed along the inner rim of the Morella basin. Dark-toned plains are distributed  
321 adjacent north of a large depression called Ganges Cavus located at the southern part of  
322 the basin and also in the areas close to the spillway (**Fig. 8**). High-resolution images  
323 of the plains reveal dark-toned materials that are relatively flat-lying and are  
324 characterized, at least locally, by their margins raised above the adjacent basin floor  
325 (positive relief) (**Fig. 9b**). Moderately dark-toned (or moderately light-toned) plains  
326 with varying shades are distributed in the central part of the basin. Some of the plains  
327 are as dark as the plains adjacent north of Ganges Cavus. THEMIS infrared data  
328 indicate that the dark-toned plains adjacent north of Ganges Cavus and in the areas  
329 close to the spillway are lighter in the daytime image but darker in the nighttime image  
330 in comparison to their surrounding Morella floors (**Fig. 10**). Thus these dark-toned  
331 plains are probably filled or covered with materials that have relatively low thermal  
332 inertia values compared with the materials of the surrounding floors. In comparison,  
333 the light-toned unit exposed in the northwestern and also northeastern parts of the basin  
334 seems to have materials with relatively high thermal inertia values. The moderately

335 dark-toned central basin plains probably have materials with intermediate thermal  
336 inertia values.

337 There are dark-toned materials observed in shallow, relatively narrow (<500 m)  
338 channels that are carved in the light-toned unit in both the northeastern and  
339 northwestern parts of the basin (**Figs. 8, 9c**). These channels originate from the rim  
340 area or from the terraces. In the moderately dark-toned plains in the central part of the  
341 basin, there are dark-toned materials that appear to be emplaced in shallow, relatively  
342 wide (up to several kilometers) channels (**Fig. 8**). These channels do not exhibit  
343 clearly-defined banks but are characterized by quasi-dendritic patterns following  
344 topographic lows. The dark-toned materials in both the narrow and wide channels are  
345 dark in visible images (both HRSC and THEMIS VIS), light in THEMIS infrared  
346 daytime images and dark in infrared nighttime images (**Figs. 8, 9c, 10**), similar in their  
347 visible and infrared (albedo and thermal inertia) properties to the materials occurring in  
348 the plains adjacent north of Ganges Cavus and in the areas close to the spillway. Some  
349 dark-toned materials of the channels appear to show their margins as positive relieves  
350 instead of simply filling in low topographies edge to edge. The lower terminations of  
351 the narrow and wide channels are delineated at two near-uniform elevation levels at  
352 1200 m and 1120 m respectively (**Fig. 11a**), elevations chosen to maximize the fitting of

353 channel terminations.

354 Ganges Cavus is ~5 km deep (**Fig. 7**), which is equivalent to the depths of nearby  
355 Ganges Chasma. Layering is exposed in the top most inner walls of the cavus, but  
356 talus materials cover lower walls (**Fig. 8**). The bottom of the cavus is relatively flat,  
357 accumulating slope-derived deposits and dark dunes. We note that the dark dunes have  
358 characteristics similar in albedo and thermal inertia to those of the dark-toned materials  
359 in the Morella basin plains and in the channels (**Figs. 8, 10**). In addition, the wind  
360 direction inferred from slip faces of the dark dunes is from NNW, implying that at least  
361 part of the dune materials was derived from the dark-toned materials on the Morella  
362 basin floor. The sediment-transporting wind initiates flow separation (Bourke et al.,  
363 2004) at the upwind wall of Ganges Cavus and probably deposits the sediments on the  
364 cavus floor. A group of elongated, low-profile hills are observed in the southeastern  
365 part of the Morella basin floor between Ganges Cavus and the spillway (**Figs. 8, 10**).  
366 A crater named Johnstown characterized by its irregular rim is located to the north of  
367 these hills. We identified a small channel originating from a shallow depression  
368 outside of the Morella basin southwest rim (**Fig. 9d**).

369 The OMEGA analysis reveals interesting results for the Morella basin (**Fig. 11b, 11c,**  
370 **11d**). Our detailed co-registration work of the OMEGA maps (derived from orbit

0394\_2) covering the western two-third of the basin and the HRSC image found good correlations between some mineral occurrences and geological units. Pyroxene is concentrated in the dark-toned plains adjacent north of Ganges Cavus and in moderately dark-toned north-central basin plains. Although the spatial resolution of the OMEGA data we used does not permit to study the composition of the dark-toned materials observed in the wide channels of the central basin area, a recently released Compact High Resolution Imaging Spectrometer (CRISM) data set (image number FRT000083F4) confirms that they are enriched in pyroxene. In addition, areas with enhanced pyroxene concentrations are apparent on the bottom of Ganges Cavus (**Fig. 11b**), and one of the areas corresponds to dark dunes. Pyroxene is distributed also outside of the Morella basin. The floor of the Morella basin is enriched in olivine minerals, both forsterite and fayalite, and their presence outside of the basin is not confirmed either because they do not exist or their presence is under the instrumental detection limits (**Fig. 11c, d**). Their distribution patterns in the basin are broadly consistent with that of olivine mapped by the OMEGA team (Mustard et al., 2005). Olivine minerals appear to be highly enriched in the light-toned basin unit distributed in the northwest part of the basin and moderately enriched in moderately dark-toned west-central basin plains. Their distributions in the central basin area do not coincide

389 well with that of pyroxene. The olivine minerals are not detected in the dark-toned  
390 plains adjacent north of Ganges Cavus. Hydrated mineral absorptions centered at  
391 around 1.9  $\mu\text{m}$  are not detected in the Morella basin.

392 *Interpretations:* The highest elevation indicative of spillover is  $\sim 1780$  m according to  
393 Coleman et al. (2007) based on a small cross-over channel (**Fig. 8**). At the 1780-m  
394 level, the topographic contour line does not close within the Morella basin on the east  
395 side. Degradation of the rim during the flooding or after disappearance of a paleolake  
396 at 1780 m may explain this situation. The MOLA grid data indicate that the range of  
397 1460–1480 m is the elevation at the spillover gap that was most likely resulted from  
398 flood incision. However, this elevation may be a false artifact overestimated by  
399 smoothing effect of interpolation in an area without MOLA tracks as pointed by  
400 Coleman et al. (2007). They instead measured elevations of the Morella floor west of  
401 the gap (1230 m) and of the Elaver Vallis floor east of the gap (1250 m) respectively,  
402 and consider that the 1250-m level represents the final outflow elevation. We adopted  
403 this spillway elevation and estimated the volume of the paleolake (**Table 1**). The  
404 volume of Ganges Cavus, which may or may not have been part of the paleolake, was  
405 estimated separately. The paleolake volume for 1780 m was also estimated assuming  
406 that the topographic contour closes at this level (**Table 1**). The lake draining from the

407 Morella basin must have been a powerful event. Indeed, the grooved morphology  
408 observed inside the Morella basin near the spillway testifies for the high-energy nature  
409 of the spillover event (**Figs. 8, 9a**). The probable maximum volume of the paleolake  
410 above the final spillway elevation (1250 m) assuming the elevation level of 1780 m was  
411 estimated, and it is  $\sim 2396 \text{ km}^3$ . This value is nearly equivalent to the volume of the  
412 Glacial Lake Missoula ( $2184 \text{ km}^3$ ; Clark et al., 1984), but much lower than the volume  
413 of water available for the Ma'adim flooding from the Eridania basin ( $100,000 \text{ km}^3$ ;  
414 Irwin et al., 2002). Thus, the maximum volume of water available for the Elaver Vallis  
415 flooding was likely similar to that of the Glacial Lake Missoula flooding. But the  
416 exact process of the spillway downcutting in the Morella basin rim could have been  
417 considerably different from that of ice-dam failure associated with the Glacial Lake  
418 Missoula flooding.

419 We note that no convincing observations, such as deltaic bodies and wave-cut  
420 terraces, indicative of a long-lasting stable paleolake exist in the Morella basin. The  
421 discontinuous chain of degraded terraces may mark a shoreline formed by modification  
422 of these features due to construction and erosion of wave action, but alternative  
423 interpretations are that they represent either slumped inner rim materials or  
424 impact-excavated lower strata of a multi-layered crust. However, the Morella basin

425 may record other lines of evidence for a paleolake of at least temporal presence as  
426 indicated by the lower terminations of channels, which are interpreted to be shorelines  
427 separating incoming fluid and a standing body of water. We estimated volumes of the  
428 purported paleolake reconstructed from the elevations of the possible shorelines at 1200  
429 m and 1120 m (**Fig. 11a**) assuming that the topography of the Morella basin has not  
430 changed drastically since the paleolake formation (**Table 1**).

431 The dark-toned plains adjacent north of Ganges Cavus are encompassed by the  
432 possible 1120-m shoreline level and are enriched in pyroxene with no olivine minerals  
433 detected. The light-toned unit exposed in the northwestern part of the basin has high  
434 concentrations of olivine minerals but pyroxene is not detected, and its lower elevation  
435 boundary coincides fairly well with the possible 1200-m shoreline level. In the  
436 moderately dark-toned plains of the central basin area, both pyroxene and olivine are  
437 detected but their distributions do not overlap well. The dark-toned materials observed  
438 in the channels with their terminations at two elevation levels (1200 m, 1120 m) are  
439 similar in albedo and thermal inertia to the pyroxene-rich dark-toned materials on the  
440 Morella basin floor. Some of them are also enriched in pyroxene as the CRISM data  
441 set indicates.

442 Multiple interpretations are plausible for explaining the above-mentioned

443 observations. 1) The pyroxene-rich dark-toned materials stratigraphically underlie the  
444 olivine-rich materials, and the former were exposed on the surface by fluid and wind  
445 erosion. We cannot totally rule out this hypothesis, but it is difficult to explain why the  
446 pyroxene-rich dark-toned materials occur in channels and topographic lows at variable  
447 elevations. 2) The pyroxene-rich dark-toned materials were likely emplaced over the  
448 olivine-rich materials by fluvial and lacustrine processes, represented by the dark-toned  
449 channels and the dark-toned plains respectively. In the central part of the basin, the  
450 emplacement was likely partial, leaving some olivine-rich materials exposed. In this  
451 scenario, the distributions of the pyroxene-rich dark-toned materials could reflect that  
452 either they are leftover sediments, consisting of relatively fine-grained particles, of the  
453 Elaver flooding and/or of the receding paleolake, or influx of materials occurred from  
454 the surrounding crater rim, for example by springs, into the paleolake. The  
455 positive-relief property of the dark-toned materials may be due to erosional processes  
456 that modified their margins. However, layering, typical of fluvial and lacustrine  
457 sediments, is not observed in the examined high-resolution images (e.g., **Fig. 9b**). 3)  
458 The pyroxene-rich dark-toned materials are eolian or volcanic deposits that filled in  
459 channels and topographic lows, or are superficial eolian or volcanic deposits that  
460 constitute the topmost part of sediments filling in channels and topographic lows. The

461 eolian interpretation of 3) may be consistent with the fact that the dark-toned materials  
462 on the Morella basin floor are similar to the dark dunes on the bottom of Ganges Cavus  
463 in albedo and thermal inertia (**Figs. 8, 10**) and also the observation of pyroxene  
464 detection in the area of the dark dunes (**Fig. 8, 11b**). However, no well-developed  
465 eolian bedform (equivalent of the dark dunes on the bottom of Ganges Cavus) occurs in  
466 the dark-toned materials on the Morella basin floor, and their eolian interpretation  
467 remains unconfirmed. The positive-relief property of the dark-toned materials may be  
468 a primary depositional form resulted from high-yield strength materials such as lava  
469 flows. However, it is also difficult to confirm the volcanic interpretation of 3) since  
470 there are no clear indications of volcanic processes such as volcanic edifice, lava  
471 morphology, and layering of pyroclastic flow deposits on the Morella basin floor.

472 The current olivine mineral distributions on the floor of the Morella basin raise two  
473 questions: 1) how they formed; 2) if alteration of the olivine minerals due to the  
474 hypothesized extensive hydrological activities, represented by the paleolake formation,  
475 occurred. Olivine is rich in magmatic rocks of mafic and ultramafic varieties. It is  
476 possible that the purported Morella impact event excavated the Martian crust and  
477 exposed olivine-rich layers. Alternatively, the basin was filled by olivine-rich volcanic  
478 materials after the formation of the basin but before the paleolake formation. Other

479 olivine-rich units were discovered in eastern Ganges Chasma by THEMIS observation  
480 (Christensen et al., 2003), and because olivine is unstable in aqueous conditions it was  
481 argued that 1) significant subsurface weathering did not occur in this region, or 2)  
482 significant surface weathering has not occurred since these units were exposed. The  
483 most plausible explanation for its survival in the Morella basin floor is that the time  
484 scale for the extensive hypothesized hydrological activities was too short to cause  
485 appreciable alteration although it is difficult to quantify the length of the time. Such  
486 scenario may also explain the absence of detected hydrated minerals in the area at least  
487 with the OMEGA spatial resolution.

488 We point out a possibility that the olivine-rich materials were formed by magmatic  
489 processes during the possible dry period lasting up until today after the last paleolake  
490 event. This scenario explains the survival of olivine minerals. However,  
491 non-aqueous processes of channel formation and emplacement of the dark-toned  
492 materials during the dry period may need to be accounted for. The channel formation  
493 could still be attributed to aqueous processes but of limited extent, such as localized  
494 springs, in order to avoid alternation of the olivine minerals. In this scenario, the  
495 pyroxene-rich dark-toned materials may have been brought in the Morella basin floor  
496 by wind from the outside or produced locally by magmatic processes.

497 Finally, non-aqueous origins such as the CO<sub>2</sub> outburst hypothesis (Hoffman, 2000)  
498 for Elaver Vallis may explain the survival of olivine minerals in the Morella basin. As  
499 mentioned earlier, the validity of such hypothesis has not been accepted. It remains to  
500 be investigated if the olivine survival is related to its existence in a non-aqueous  
501 environment.

502

## 503 **5. Allegheny Vallis, Walla Walla Vallis, and paleolake formation in a** 504 **40-km-diameter basin**

505

### 506 *5.1. Allegheny Vallis, an outflow channel system*

507

508 *Observations:* In Ophir Planum, Allegheny Vallis originates from a 1800-m-deep  
509 elongated depression called Ophir Cavus (**Fig. 12**) (Dinwiddie et al., 2004). Terraces  
510 are observed at the upper reach of Allegheny Vallis (**Fig. 13a**), and layered outcrops  
511 occur on the bottom of Ophir Cavus (**Fig. 13b**). The uppermost layer of these outcrops  
512 in Ophir Cavus appears to be light toned. A northern tributary of Allegheny Vallis  
513 originates from small depressions (**Figs. 12, 13c**). The Allegheny Vallis system is  
514 slightly longer than Elaver Vallis but narrower in width. It is ~200 km long and the

515 maximum width is 15–25 km at its expanded reaches (**Fig. 12**). Allegheny Vallis’  
516 middle reach is anastomosing and exhibits a complex pattern of scablands (Coleman et  
517 al., 2007). Longitudinal grooves are developed on some parts of its floors. At its  
518 middle reach, the channel cuts across a low north-south-trending ridge (**Fig. 12**) that is  
519 interpreted to be part of a wrinkle ridge system concentric to the Tharsis bulge (e.g.,  
520 Wise et al., 1979; Mège and Masson, 1996b). Expansion of the reach is observed after  
521 the breaching of the wrinkle ridge (**Fig. 12**). A deep V-shaped canyon with theater-like  
522 heads is observed in the expanded lowermost reach of Allegheny Vallis (**Fig. 12**).

523 *Interpretations:* The morphological characteristics, in addition to its large-scale  
524 dimensions, make it possible to classify Allegheny Vallis as an outflow channel system  
525 formed by cataclysmic flooding, probably of water. Either single or multiple flooding  
526 is envisaged for its formation, and the terraces (**Fig. 13a**) could have resulted from  
527 waning of single flood or from multiple floods. The discharge rate range for  
528 Allegheny Vallis was estimated by Coleman et al. (2007) to be  $0.7\text{--}3 \times 10^6 \text{ m}^3 \text{ s}^{-1}$  with  
529 an assumed water depth range of 30–60 m. This value range is in general significantly  
530 lower than the estimated discharge rate range for Elaver Vallis ( $10^6\text{--}10^8 \text{ m}^3 \text{ s}^{-1}$ ), but it is  
531 explainable mainly because 1) Elaver Vallis is deeper and wider than Allegheny Vallis,  
532 2) a bankfull discharge assumption was applied for estimating the upper limit of flow

533 depth in the Elaver Vallis calculation, but not for Allegheny Vallis. Other parameters  
534 such as energy slope and Manning coefficient used in the two estimations are essentially  
535 the same.

536 The cross-cutting relationship indicates that the channel formation postdates that of  
537 the wrinkle ridge. The terminal deep V-shaped canyon is similar to the terminal  
538 V-shaped canyon associated with Elaver Vallis, and groundwater sapping/debris flow  
539 processes after the flooding were probably responsible for its formation.

540

## 541 5.2. Walla Walla Vallis

542

543 *Observations:* Wallula, a crater basin approximately 12 km in diameter is pierced by  
544 Walla Walla Vallis. Walla Walla Vallis (~40 km long) (**Figs. 12, 14**) is connected with  
545 a pit-crater chain to the south of the crater basin. Another channel originating from  
546 Ophir Cavus and merging with Walla Walla Vallis was noted by Dinwiddie et al. (2004).  
547 The floor of the Wallula basin is filled with a dark-toned deposit that seems to have its  
548 eastern margin raised above the basin floor. This positive-relief property is similar to  
549 that of the dark-toned materials on the Morella basin (**Fig. 9b**). A channel segment of  
550 Walla Walla Vallis is carved on this deposit (**Fig. 14**).

551 *Interpretations:* The system of Walla Walla Vallis and the Wallula basin was first  
552 studied by Dinwiddie et al. (2004), and they suggested it to have sourced water from the  
553 pit-crater chain. The dark-toned deposit in the Wallula basin seems to have been  
554 transported, at least partially through Walla Walla Vallis, from the pit-crater chain.  
555 This is consistent also with the fact that similar dark-toned materials are observed also  
556 in the vicinity of the pit-crater chain (**Fig. 14**). Two interpretations are possible for the  
557 origin of the dark-toned deposit: 1) the fluid emerged from the pit-crater chain and  
558 transported to the Wallula basin was a water-sediment mixture such as  
559 hyperconcentrated flow or debris flow; 2) the dark-toned deposit consists of volcanic  
560 materials derived from the pit-crater chain, which is a hypothesis similar to the one  
561 proposed in western Memnonia (Leverington and Maxwell, 2004).

562

### 563 *5.3. Paleolake in a 40-km-diameter basin*

564

565 *Observations:* An unnamed crater basin 40 km in diameter east of Wallula exhibits a  
566 fan-shaped deposit at the mouth of a short valley cutting into the rim on its northeastern  
567 section (**Fig. 15a**). The lower larger fan's external geometry is characterized by a  
568 broadly flat, low-gradient top portion and steep front slopes inclining towards the basin.

569 Layers are visible at the front slopes (**Fig. 15b**). A smaller, much thinner multi-leveled  
570 fan complex is superposed on top of the lower fan (**Fig. 15b**). The valley behind the  
571 fan-shaped deposit has somewhat unusual morphology for a fluvial valley: it consists of  
572 two quasi-circular depressions along its long axis (**Fig. 15a**). An elongated depression  
573 is carved in the southern rim of this basin, and a small valley is incised into a massif  
574 east of the basin (**Fig. 15a**).

575 *Interpretations:* The external geometry of the fan-shaped deposit is similar to what is  
576 often observed with a deltaic body called Gilbert-type delta, thus it is likely a fan delta  
577 (Di Achille and Komatsu, 2008). Gilbert-type deltas commonly occur on Earth  
578 (Gilbert, 1890), and possible Gilbert-type deltas have been found elsewhere on Mars  
579 (e.g., Ori et al., 2000). The layers observed at the front slopes imply vertical stacking  
580 of sediments or erosional exposure of sediments deposited by progradation. Two  
581 interpretations are possible for the observation of the lower fan and the thinner  
582 multi-leveled fan complex: 1) the lower fan formed first with a larger amount of  
583 sediment supply, and the upper fan formed later with a smaller amount of sediment  
584 supply; 2) the lower fan and the upper fan together formed a fan delta that was later  
585 eroded to form multiple scarps, which is an interpretation similar to that of a multi-level  
586 fan complex at the mouth of Tyras Vallis (Di Achille et al., 2006).

587 The presence of a fan delta indicates that this basin was inundated by fluid, most  
588 likely water, sometime in the past. The elevation of the main delta front (~1300 m)  
589 coincides with channel termini of the centripetal drainage system positioned inward of  
590 the rim (Di Achille and Komatsu, 2008) (**Fig. 15a**). This level most likely represents a  
591 paleolake surface.

592

## 593 **6. Discussion**

594

### 595 *6.1. Emergence of water from Ganges and Ophir cavi, and other smaller depressions*

596

597 With the scarcity of observed impact craters within 5-km-deep Ganges Cavus  
598 possibly due to slope failures of its steep walls and accumulations of mass-wasting  
599 materials on the bottom, establishing the age relationship between this depression and  
600 other geological units is a difficult task. The timing of the Ganges Cavus formation  
601 could have been 1) before the formation of the purported paleolake, 2) concurrent with  
602 the paleolake, or 3) after the disappearance of the paleolake. We argue that Ganges  
603 Cavus, not necessarily at its present geometry, was possibly a source of water that filled  
604 the Morella basin up to over 1700 m. Precipitation in the area may not be ruled out as

605 the source of water in the basin. In fact, the formation of dendritic valleys found near  
606 Echus and Melas chasmata of the Valles Marineris system has been attributed to  
607 precipitation (Mangold et al., 2004; Quantin et al., 2005). However, no clear  
608 occurrence of similar fluvial valleys in the areas of Aurorae and Ophir plana has been  
609 noted to date. This does not necessarily exclude the precipitation hypothesis, but it is  
610 uncertain in these areas. This leaves groundwater rising through, but not restricted to,  
611 Ganges Cavus as the probable mechanism of water supply within the Morella basin.  
612 This view is consistent with Coleman et al. (2003, 2007) and Coleman and Dinwiddie  
613 (2007), who interpreted Ganges Cavus as being undermined and excavated by the  
614 eruption of confined groundwater. Emergence of groundwater is envisaged also in the  
615 cases of chaos-originated outflow channels that are common in the circum-Chryse  
616 region (Rotto and Tanaka, 1995) or of fracture-originated outflow channels (e.g., Burr et  
617 al., 2002; Ghatan et al., 2005). The channels observed in the Morella basin floor (**Fig.**  
618 **8**) indicate that water may have emerged not only from Ganges Cavus but also from  
619 many other localized small-scale springs with in the basin.

620 The water emerging from Ganges Cavus may have rapidly or slowly filled the  
621 Morella basin. After the paleolake reached the initial spillover elevation, a large  
622 quantity of water was drained to Elaver Vallis through the spillway, and the peak

623 draining rate was high as indicated by the grooves near the spillway (**Figs. 8, 9a**). We  
624 note that in the case of the multiple-flood hypothesis, the incision of the spillway gap  
625 continued over multiple floods resulting from multiple infilling episodes of the Morella  
626 basin. It is also possible that the cycle of the Morella paleolake formation and total  
627 disappearance occurred more than once. The stabilization of the paleolake after the  
628 Elaver flooding probably occurred at the elevation of the spillway (~1250 m) (**Figs. 8,**  
629 **11a**). The lower terminations of channels at 1200 m and 1120 m may record paleolake  
630 levels in the Morella basin during the receding phase (**Figs. 8, 11a**). The morphologies  
631 of the elongated hills (**Figs. 8, 10**) observed in the area between Ganges Cavus and the  
632 spillway, and Johnstown, a probable degraded impact crater, may be related to the  
633 movement of water during the emergence from Ganges Cavus, the cataclysmic draining  
634 to Elaver Vallis, or the receding phase of the remaining paleolake.

635 The cataclysmic nature of the spillover from a crater lake may be explained by rapid  
636 incision/failure of the crater rim and consequent increase of discharge. Both of these  
637 factors have a feedback on each other, further increasing the scale of flooding. We  
638 note that possible rapid emergence of water from Ganges Cavus itself could have also  
639 contributed to the high-discharge flood flows. In the case of Allegheny Vallis, the  
640 source of the flooding was clearly Ophir Cavus. And the cataclysmic nature of the

641 flooding requires that water had to come out of the cavus rapidly.

642 In addition to Ganges and Ophir cavi, other smaller depressions exhibit evidence for  
643 water emergence. For example, Walla Walla Vallis and the Wallula basin appear to  
644 have received a water-sediment mixture from a pit-crater chain to the south, although  
645 we cannot rule out volcanic origin for the observed features. Both the pit-crater chain  
646 and Walla Walla Vallis are an order of magnitude smaller than Ophir Cavus and  
647 Allegheny Vallis respectively, implying a much smaller scale of water emergence. The  
648 small channel to the southwest of the Morella basin (**Fig. 9d**) and the branch of  
649 Allegheny Vallis also originate from shallow depressions (**Fig. 13c**).

650 The evidence for water emergence from depressions to explain the hypothesized  
651 ponding within the 40-km-diameter basin is less certain but it is a possibility (**Fig. 15a**).  
652 The local elevation level of 2550 m (**Fig. 16b**) indicates that the floodwater of  
653 Allegheny Vallis may have inundated and ponded in the plains near Ophir Cavus at least  
654 temporarily before deep incision, consistent with the inference by Coleman et al. (2007).  
655 The valley behind the possible fan delta or its ancestral valley was likely a conduit for  
656 the water flowed from the plains. Thus, one possible scenario is that the Allegheny  
657 Vallis floodwater flowed into the basin, forming a paleolake and the fan delta. Water  
658 may have been provided also through the small valley incised into a massif east of the

659 basin from other unidentified source (**Fig. 15a**). Another possibility to be considered  
660 is that the water originated within the valley behind the fan delta, where the two  
661 quasi-circular depressions comprising the valley are morphologically similar to the  
662 pit-crater chain from which water emerged and flowed into the Wallula basin (**Fig. 14**).  
663 We point out that the elongated depression carved in the southern rim of this basin and  
664 localized small-scale springs feeding the centripetal drainage system may have been  
665 alternative or additional sources of water (**Fig. 15a**).

666 If the hypothesized hydrological activities occurred during the period(s) of no or  
667 limited cryosphere development, the water may have emerged in various depressions  
668 and crater basins by regional groundwater table rising. Water may have also emerged  
669 as springs or seepages from various locations in Aurorae and Ophir plana, filling in  
670 depressions and crater basins. But this mechanism may not explain some observations  
671 indicating rapid emergence of water from depressions (e.g., Ophir Cavus and possibly  
672 Ganges Cavus).

673 Spring mechanism has been proposed to explain interior layered deposits (i.e.,  
674 light-toned deposits) in Valles Marineris (Rossi et al., 2008), and emergence of water  
675 may have been common also in Aurorae and Ophir plana. Recent detection of  
676 silica-rich alteration products (SiOH-bearing phases) in finely-layered strata distributed

677 in the plains surrounding Valles Marineris chasmata (Le Deit et al., 2008; Milliken et al.,  
678 2008) is generally consistent with our view that these plains experienced extensive  
679 hydrological processes in the past. However, the timings for all these hydrological  
680 events are unknown.

681

## 682 *6.2. Water releasing mechanisms*

683

684 Water may have been stored as both groundwater or ground ice within the crust if a  
685 cryosphere existed. However, we currently lack information on the actual depths of  
686 cryosphere on Mars, let alone in the geological past. Clifford (1993) and Clifford and  
687 Parker (2001) theoretically derived depth to the base of the equatorial cryosphere on  
688 Mars as 2.3–11 km, 2.3–4.7 km, respectively. In comparison, depths of the cavi  
689 identified in our study area as water sources are: Ganges Cavus, ~5 km; Ophir Cavus,  
690 1800 m. If emergence of water from Martian crust requires melting of ground ice or  
691 breaching of cryosphere to release water from the underlying hydrosphere, the great  
692 depths of the cavi and their isolated nature indicate that melting of cryosphere was  
693 intensive but nonetheless localized.

694 Pit-crater chains on Mars were extensively studied by Wyrick et al. (2004). They  
695 concluded that dilational normal faulting and sub-vertical fissuring provide a simple and  
696 comprehensive mechanism for their development. They pointed out that pit-crater  
697 chains and the underlying dilational faults or fissures, may provide pathways for magma,  
698 although dikes and magma chambers are not necessarily required for formation of the  
699 pit-crater chains. The pit-crater chains in Ophir Planum are hypothesized to have  
700 formed over intruding dikes (Schultz, 1989; Okubo and Schultz, 2005). This  
701 hypothesis is consistent with the emergence of water from these pit craters since the  
702 magmatic heat in the Valles Marineris region (e.g., McKenzie and Nimmo, 1999) could  
703 have melted ground ice or, as a consequence of the melting, released groundwater  
704 stored underneath the cryosphere in the crust. Similarly, interaction of rising dikes and  
705 the Martian hydrosphere and its consequent pit or chaos formation were discussed  
706 previously (e.g., Mège and Masson, 1996c; Meresse et al., 2008). Thus we consider  
707 dike intrusion to be an important cause of formation for the cavi and smaller  
708 depressions in Aurorae and Ophir plana, explaining also melting of ground ice or  
709 breaching of cryosphere. Wrinkle ridges and underlying faults have been proposed as  
710 local sources of water in southwestern Chryse Planitia (Rodriguez et al., 2007).

711 Wrinkle ridges occur widely in Ophir Planum but there is no clear evidence of water  
712 emergence from these features at least within our observation.

713 The emergence of water from cavi or smaller depressions may be complicated if the  
714 volatiles in the crust are not only water but also CO<sub>2</sub>. The system of H<sub>2</sub>O-CO<sub>2</sub>  
715 produces clathrate hydrate at certain ranges of pressure and temperature in Martian crust.  
716 Under the inferred Martian crustal conditions, clathrate hydrate may coexist with water  
717 ice, dry ice, liquid water, liquid CO<sub>2</sub>, depending on the ratio between H<sub>2</sub>O and CO<sub>2</sub> (e.g.,  
718 Rodriguez et al. 2006). Below the depths of clathrate dissociation, two liquids (H<sub>2</sub>O  
719 and CO<sub>2</sub>) could coexist immiscibly. The north-trending alcove-shaped depression  
720 called Ganges chaos (**Figs. 1, 16a**), located ~250 km east of the Morella basin, was  
721 proposed by Rodriguez et al. (2006) to have evolved by clustering of chaotic terrains  
722 formed by depressurization-induced or thermally-triggered dissociation of buried gas  
723 clathrate hydrates and explosive eruption of gas-saturated groundwater. Furthermore,  
724 the cataclysmic emergence of water by this mechanism for both CO<sub>2</sub> and CH<sub>4</sub> hydrates  
725 was proposed for the genesis of chaotic terrains and outflow channels (e.g., Komatsu et  
726 al., 2000; Max and Clifford, 2000) east of Ganges Chasma (**Fig. 1**). A similar process  
727 involving clathrate hydrate may have operated also at Ganges and Ophir cavi, and other  
728 smaller depressions.

729       Recent spectral identification of hydrous sulfates in nearby Gangis Chasma  
730 (Quantin et al., 2006) may indicate another mode of water release in the region.  
731 Montgomery and Gillespie (2005) proposed that in Tharsis increased temperatures  
732 adequate to dehydrate hydrous evaporites would trigger significant volumetric  
733 expansion and cataclysmically release tremendous amounts of overpressured water.  
734 This process produces a water-dehydrated salt mixture that expands volumetrically over  
735 the original hydrous salt (as much as over 50%). This mechanism possibly explains  
736 the emergence of water from the cavi and other smaller depressions. We note that the  
737 hypothesis of a “mega-slide” driven by constinental-scale salt tectonics to explain  
738 Valles Marineris chasmata (Montgomery et al., 2009) provides a mechianism for  
739 discharging at the margin of the deforming area, including Aurorae and Ophir plana.

740       Although the examined OMEGA data do not present evidence for hydrous sulfates  
741 in Aurorae and Ophir plana at their spatial resolutions, the bright layered materials at  
742 the bottom of Ophir Cavus could contain such minerals or dehydrated salts. The spatial  
743 resolution of spectral instrument is important in determining the detection potential of  
744 salt minerals (e.g., Komatsu et al., 2007), thus it needs to be investigated with higher  
745 spatial-resoulution spectral data such as those acquired by CRISM.

746

747 6.3. Groundwater migration through fractures and/or caverns

748

749 A mechanism for explaining the emergence of large quantities of water and  
750 consequent hydrological activities in Aurorae and Ophir plana (**Fig. 16b**) probably  
751 involves crustal migration of the water. It is possible that the water stored in the  
752 terrain >2500 m above the Martian datum may have emerged from depressions in Ophir  
753 Planum as proposed by Coleman et al. (2007). Locations of Ophir and Ganges cavi,  
754 and also other smaller depressions are approximately in line with subsidence features  
755 such as Ophir Catenae and large canyons of Candor Chasma (**Fig. 16a**). All the  
756 depressions also have approximate east-west orientations, being concordant with  
757 orientations of fractures radial to the Tharsis bulge (e.g., Wise et al., 1979).  
758 Furthermore, these depressions have an echelon alignment (**Fig. 2**). This echelon  
759 alignment noted also in earlier works (e.g., Schultz, 1989; Mège and Masson, 1996a;  
760 Coleman et al., 2007) indicates that these depressions are related to each other and there  
761 is clearly a structural control over these features. Such structural control may have  
762 been provided by dike swarms (e.g., Schultz, 1998), and the pit-crater chains may be a  
763 surface expression of laterally propagating subsurface dikes or hydrofractures (Schultz,  
764 1989). Therefore one cause of water emergence from Ophir and Ganges cavi, and

765 other smaller depressions is related to long-range (hundreds of kilometers)  
766 structurally-controlled groundwater migration. Past groundwater activities at some  
767 sites of Mars, particularly in the region stretching from Arabia Terra to Valles Marineris,  
768 are hypothesized based on mineralogy (e.g., Geissler et al., 1993; Chan et al., 2004;  
769 McLennan et al., 2005), morphology (e.g., Ormö et al., 2004; Treiman, 2008; Rossi et  
770 al., 2008), or halos along fractures (Okubo and McEwen, 2007; Okubo et al., in press).  
771 Thus groundwater activities on Mars may have been wide spread.

772 We hypothesize that a large volume of groundwater originated in higher plains areas  
773 in western Ophir Planum migrated through a system of subsurface fractures and/or  
774 caverns (**Fig. 16**). The water eventually emerged in Ophir and Ganges cavi, and other  
775 smaller depressions, and even in crater basins. The western plains areas were  
776 proposed to have been where water originated, and an ice-covered paleolake in Candor  
777 Chasma further west may have been another source of water (Coleman et al. 2003,  
778 2007). Groundwater may have been stored in confined aquifers, or water ice may  
779 have melted owing to magmatic heating or climatic change. The groundwater can also  
780 migrate through a permeable crustal medium, but a presence of fractures and/or caverns  
781 enhances and focuses water mobility. Migration of water would be greatly increased if  
782 caverns exist: a cavern system was envisaged between Ganges Chasma and the

783 Shalbatana Vallis headwater source (**Fig. 1**) (Rodriguez et al., 2003). We add that  
784 hydraulic conductivity can be enhanced also by the presence of buried impact craters in  
785 the area (Rodriguez et al., 2005a). Ground penetrating radars such as the Mars  
786 Advanced Radar for Subsurface and Ionospheric Sounding (MARSIS) and Shallow  
787 Subsurface Radar (SHARAD) may provide data that confirm or reject such hypotheses.

788 How the crustal water (in liquid or ice form) had become enriched to cause the  
789 hydrological activities observed in Aurorae and Ophir plana has to be explained.  
790 Climatic shift is a possible mechanism for both deposition of water on the surface and  
791 recharging of aquifers. For example, snowpacks or glaciers on the Tharsis rise, formed  
792 during periods of high obliquity when precipitation occurs at low latitudes (e.g.,  
793 Jakosky and Carr, 1985; Abe et al., 2005) have been suggested to be an efficient source  
794 of recharge and may have provided hydraulic head for the circum-Chryse outflow  
795 channels (Harrison and Grimm, 2004; Russell and Head, 2007). This mechanism could  
796 have stored crustal water necessary also for the hydrological activities observed in  
797 Aurorae and Ophir plana (Coleman et al., 2007).

798

## 799 **7. Conclusions**

800

801 Aurorae and Ophir plana south and west of Ganges Chasma are found to be regions  
802 characterized by ancient hydrological processes including formation of paleolakes and  
803 paleo-flood channels. Ganges Cavus is a 5-km-deep depression of probable collapse  
804 origin located within the Morella crater basin in Aurorae Planum. A paleolake(s) in  
805 the Morella basin likely formed by water emergence at least partially through Ganges  
806 Cavus or its incipient depression. Water may have been supplied also from small-scale  
807 springs within the basin. Cataclysmic spillover occurred, breached the eastern rim,  
808 and formed an outflow channel system called Elaver Vallis. Multiple levels of the  
809 paleolake in the Morella basin are inferred from possible shoreline features. Ophir  
810 Planum, plains unit west of the Morella basin, hosts another outflow channel system  
811 called Allegheny Vallis that originates from 1800-m-deep depression Ophir Cavus.  
812 The nearby Wallula crater basin may have received water from a pit-crater chain to its  
813 south. An unnamed crater basin 40 km in diameter to the south of Allegheny Vallis  
814 seems to have hosted a paleolake as inferred from the presence of a possible fan delta  
815 formed on the basin floor. Water may have been derived from outside of the basin, or  
816 it may have emerged from depressions on its rim and/or small-scale springs within the  
817 basin.

818 Water emergence in Aurorae and Ophir plana may have occurred as consequences  
819 of ground ice melting or breaching of cryosphere to release water from the underlying  
820 hydrosphere. Dike intrusion is considered to be an important cause of formation for  
821 the cavi and smaller depressions explaining also melting of ground ice or breaching of  
822 cryosphere. Alternatively, the depressions and crater basins may have been filled by  
823 regional groundwater table rising during the period(s) when cryosphere was absent or  
824 considerably thin.

825 The large quantities of water emerged in Aurorae and Ophir plana may have been  
826 derived from the crust of higher plains in western Ophir Planum where water existed in  
827 confined aquifers or was produced by melting of ground ice due to magmatic heating or  
828 climatic shift, or from a paleolake in Candor Chasma further west. We hypothesize  
829 that the groundwater migrated through the crust characterized by the presence of  
830 fractures and/or caverns.

831 Our work revealed that the plains near Ganges Chasma are of paramount importance  
832 for future explorations from both geological and exobiological points of view because  
833 of their diverse geological evidence for water activities in the past.

834

835 **Acknowledgements.** We thank constructive comments by Monica Pondrelli and  
836 Simone Silvestro. The reviews comments by Vic Baker and an anonymous reviewer  
837 were also helpful. All the THEMIS and MOC data are credited to NASA/JPL/Arizona  
838 State University, NASA/Malin Space Science Systems respectively. We used the  
839 HRSC data processed by HRSC view provided by Freie Universitaet Berlin and DLR  
840 Berlin. The OMEGA data are credited to ESA/IAS. This project was supported by  
841 the joint ASI/IRSPS PAGIS (Planetary Geosciences Information System) program.

842

843 **References:**

844

845 Abe, Y., Numaguti, A., Komatsu, G., Kobayashi, Y., 2005. Four climate regimes on a  
846 land planet with wet surface: Effects of obliquity change and implications for  
847 ancient Mars. *Icarus* 178, 27–39.

848 Baker, V.R., 1978. The Spokane Flood controversy and the Martian outflow channels.  
849 *Science* 202, 1249–1256.

850 Baker, V.R., 1982. *The Channels of Mars*. University of Texas Press, Austin, Texas,  
851 198 pp.

- 852 Baker, V.R., Milton, D.J., 1974. Erosion by catastrophic floods on Mars and Earth.  
853 Icarus 23, 27–41.
- 854 Baker, V.R., Benito, G., Rudoy, A.N., 1993. Paleohydrology of Late Pleistocene  
855 superflooding, Altai Mountains, Siberia. Science 259, 348–350.
- 856 Bourke, M.C., Bullard, J., Barnouin-Jha, O., 2004. Aeolian sediment transport pathways  
857 and aerodynamics at troughs on Mars. J. Geophys. Res. 109, E07005,  
858 doi:10.1029/2003JE002155.
- 859 Burr, D.M., Grier, J.A., McEwen A.S., Keszthelyi, L.P., 2002. Repeated aqueous  
860 flooding from the Cerberus Fossae: Evidence for very recently extant, deep  
861 groundwater on Mars. Icarus 159, 53–73.
- 862 Cabrol, N.A., Grin, E., 1999. Distribution, classification, and ages of Martian impact  
863 crater lakes. Icarus 142, 160–172.
- 864 Chan, M.A., Beitler, B., Parry, W.T., Ormö, J., Komatsu, G., 2004. A possible terrestrial  
865 analogue for haematite concretions on Mars. Nature 429, 731–734.
- 866 Chapman, M.G., Tanaka, K.L., 2002. Related magma-ice interactions: possible origins  
867 of chasmata, chaos, outflow channels, and surface materials in Xanthe,  
868 Margaritifer, and Meridiani Terrae, Mars. Icarus 155, 324–339.
- 869 Christensen, P.R., Bandfield, J.L., Bell, J.F., III, Gorelick, N., Hamilton, V.E., Ivanov, A.,

- 870 Jakosky, B.M., Kieffer, H.H., Lane, M.D., Malin, M.C., Mehall, G.L.,  
871 McConnochie, T., McEwen, A.S., McSween, H.Y., Jr., Moersch, J.E., Nealon,  
872 K.H., Rice, J.W., Jr., Richardson, M.I., Ruff, S.W., Smith, M.D., Titus, T.N., Wyatt,  
873 W., 2003. Morphology and composition of the surface of Mars: Mars Odyssey  
874 THEMIS results. *Science* 300, 2056–2061.
- 875 Clark, G.K.C., Mathews, W.H., Pack, R.T., 1984. Outburst floods from glacial Lake  
876 Missoula. *Quaternary Research* 22, 289–299.
- 877 Clifford, S.M., 1993. A model for the hydrologic and climatic behavior of water of Mars,  
878 *J. Geophys. Res.* 98, 10,973–11,016.
- 879 Clifford, S.M., Parker, T.J., 2001. The evolution of the Martian hydrosphere:  
880 Implications for the fate of a primordial ocean and the current state of the northern  
881 plains. *Icarus* 154, 40–79.
- 882 Coleman, N.M., 2003. Aqueous flows carved the outflow channels on Mars. *J. Geophys.*  
883 *Res.* 108, doi:10.1029/2002JE001940.
- 884 Coleman, N.M., 2005. Martian megaflood-triggered chaos formation, revealing  
885 groundwater depth, cryosphere thickness, and crustal heat flux. *J. Geophys. Res.*  
886 110, E12S20, doi:10.1029/2005JE002419.
- 887 Coleman, N.M., Dinwiddie, C.L., 2007. Hydrologic analysis of the birth of Elaver Vallis,

- 888 Mars by catastrophic drainage of a lake in Morella Crater. In: Seventh  
889 International Conference on Mars, Abstract #3107.
- 890 Coleman, N.M. Dinwiddie, C.L., Casteel, K., 2003. High channels on Mars indicate  
891 Hesperian recharge at low latitudes. In Sixth International Conference on Mars, #  
892 3071.
- 893 Coleman, N.M., Dinwiddie, C.L., Casteel, K., 2007. High outflow channels on Mars  
894 indicate Hesperian recharge at low latitudes and the presence of canyon lakes.  
895 Icarus 189, 344–361, doi:10.1016/j.icarus.2007.01.020.
- 896 Di Achille, G., Komatsu, G., 2008. Using HRSC and HiRISE for the study of Martian  
897 depositional environments: an example from Ophir Planum. In: Proc. Lunar Planet.  
898 Sci. Conf. 39th, Abstract #1608.
- 899 Di Achille, G., Marinangeli, L., Ori, G.G., Hauber, E., Gwinner, K., Reiss, D., Neukum,  
900 G., 2006. Geological evolution of the Tyras Vallis paleolacustrine system, Mars. J.  
901 Geophys. Res. 111, E04003, doi:10.1029/2005JE002561.
- 902 Dinwiddie, C.L., Coleman, N.M., Necsoiu, M., 2004. Walla Walla Vallis and Wallulla  
903 Crater: two recently discovered Martian features record aqueous history. In: Proc.  
904 Lunar Planet. Sci. Conf. 35th, Abstract #1316.

- 905 Dohm, J.M., Maruyama, S., Baker, V.R., Anderson, R.C., Ferris, J.C., 2002. Evolution  
906 and traits of Tharsis superplume, Mars: Superplume International Workshop,  
907 Abstracts with Programs, Tokyo Institute of Technology, Tokyo, 406–410.
- 908 Geissler, P.E., Singer, R.B., Komatsu, G., Murchie, S., Mustard, J., 1993. An unusual  
909 spectral unit in west Candor Chasma: Evidence for aqueous or hydrothermal  
910 alteration in the Martian canyons. *Icarus* 106, 380–39.
- 911 Ghatan, G.J., Head, J.W. Wilson, L., 2005. Mangala Valles, Mars: Assessment of early  
912 stages of flooding and downstream flood evolution, *Earth, Moon, and Planets*, doi:  
913 10.1007/s11038-005-9009-y.
- 914 Gilbert, G.K., 1890. Lake Bonneville. U.S. Geological Survey Monograph 1.  
915 Washington, D.C., 438 pp.
- 916 Greeley, R., Kuzmin, R.O., Nelson, D., Farmer, J., 2003. Eos Chasma, Mars: site for  
917 astrobiology. *J. Geophys. Res.* 108, doi:10.1029/2002JE002014.
- 918 Harrison, K.P., Grimm, R.E., 2004. Tharsis recharge: A source of groundwater for  
919 Martian outflow channels. *Geophys. Res. Lett.* 31, L14703,  
920 doi:10.1029/2004GL020502.
- 921 Hartmann, W.K., 1999. Martian cratering VI: Crater count isochrones and evidence for  
922 recent volcanism from Mars Global Surveyor. *Meteoritics and Planetary Sciences*  
923 34, 167–177.

- 924 Hartmann, W.K., Neukum, G., 2001. Cratering chronology and the evolution of Mars,  
925 Space Science Reviews 96, 165–194.
- 926 Hoffman, N., 2000. White Mars: A new model for Mars surface and atmosphere based  
927 on CO<sub>2</sub>. Icarus 146, 326–342.
- 928 Howard, A.D., Moore, J.M., Irwin R.P.III, 2005. An intense terminal epoch of  
929 widespread fluvial activity in the Martian highlands: 1. Valley network incision  
930 and associated deposits. J. Geophys. Res. 110, E12S14,  
931 doi:10.1029/2005JE002459.
- 932 Irwin, R.P.III, Maxwell, T.A., Howard, A.D., Craddock, R.A., Leverington, D.W., 2002.  
933 A large paleolake basin at the head of Ma'adim Vallis, Mars. Science 296,  
934 2209–2212.
- 935 Ivanov, B.A., 2001. Mars/Moon cratering rate ratio estimates, Space Science Reviews  
936 96, 87–104.
- 937 Jakosky, B.M., Carr, M.H., 1985. Possible precipitation of ice at low latitudes of Mars  
938 during periods of high obliquity. Nature 315, 559–561.
- 939 Komar, P.D., 1979. Comparison of the hydraulics of water flows in Martian outflow  
940 channels with flows of similar scale on Earth. Icarus 37, 156–181.
- 941 Komatsu, G., Baker, V.R., 1997. Paleohydrology and flood geomorphology of a Martian  
942 outflow channel, Ares Vallis. J. Geophys. Res. 102, 4151–4160.

- 943 Komatsu, G., Baker, V.R., 2007. Formation of valleys and cataclysmic flood channels  
944 on Earth and Mars. In: Chapman, M.G. (ed), *The Geology of Mars: Evidence*  
945 *from Earth-Based Analogs*. Cambridge University Press, 297–321.
- 946 Komatsu, G., J.S. Kargel, V.R. Baker, R.G. Strom, G.G. Ori, C. Mosangini and K.L.  
947 Tanaka, 2000. A chaotic terrain formation hypothesis: Explosive outgas and  
948 outflow by dissociation of clathrate on Mars. In: *Proc. Lunar Planet. Sci. Conf.*  
949 31st, Abstract #1434.
- 950 Komatsu, G., Dohm, J.M., Hare, T.M., 2004. Hydrologic processes of large-scale  
951 tectonomagmatic complexes in Mongolia-southern Siberia and on Mars. *Geology*  
952 32, 325–328.
- 953 Komatsu, G., Ori, G.G., Marinangeli, L., Moersch, J.E., 2007. Playa environments on  
954 Earth: Possible analogues for Mars. In: Chapman, M.G. (ed), *The Geology of*  
955 *Mars: Evidence from Earth-Based Analogs*. Cambridge University Press,  
956 322–348.
- 957 Komatsu, G., Arzhannikov, S.G., Gillespie, A.R., Burke, R.M., Miyamoto, H., Baker,  
958 V.R., 2009. Quaternary paleolake formation and cataclysmic flooding along the  
959 upper Yenisei River. *Geomorphology* 104, doi:10.1016/j.geomorph.2008.08.009,  
960 143–164.

- 961 Le Deit, L., Bourgeois, O., Le Mouélic, S., Mège, D., Combe, J.-Ph., Sotin, C., Massé,  
962 M., 2008. Light-toned layers on plateaus above Valles Marineris (Mars). In: Proc.  
963 Lunar Planet. Sci. Conf. 39th, Abstract #1740.
- 964 Leverington, D.W., 2004. Volcanic rilles, streamlined islands, and the origin of outflow  
965 channels on Mars. *J. Geophys. Res.* 109, E10011, doi:10.1029/2004JE002311.
- 966 Leverington, D.W., Maxwell, T.A., 2004. An igneous origin for features of a candidate  
967 crater-lake system in western Memnonia, Mars. *J. Geophys. Res.* 109, E06006  
968 doi:10.1029/2004JE002237.
- 969 Malin, M.C., Edgett, K.S., 2003. Evidence for persistent flow and aqueous  
970 sedimentation on early Mars. *Science* 302, 1931–1934.
- 971 Mangold, N., Quantin, C., Ansan, V., Delacourt, C., Allemand, P., 2004. Evidence for  
972 precipitation on Mars from dendritic valleys in the Valles Marineris area. *Science*  
973 305, 78–81.
- 974 Max, M.D., Clifford, S.M., 2000. The initiation of Martian outflow channels through  
975 the catastrophic decomposition of methane hydrate, In: Proc. Lunar Planet. Sci.  
976 Conf. 31st, Abstract #2094.
- 977 McKenzie, D., Nimmo, F., 1999. The generation of Martian floods by melting  
978 permafrost above dykes. *Nature* 397, 231–233.

- 979 McLennan, S.M., Bell, III, J.F., Calvin, W., Christensen, P.R., Clark, B.C., de Souza,  
980 P.A., Farmer, J., Farrand, W.H., Fike, D.A., Gellert, R., Ghosh, A., Glotch, T.D.,  
981 Grotzinger, J.P., Hahn, B., Herkenhoff, K.E., Hurowitz, J.A., Johnson, J.R.,  
982 Johnson, S.S., Jolliff, B.L., Klingelhöfer, G., Knoll, A.H., Learner, Z.A., Malin,  
983 M.C., McSween, Jr, H.Y., Pockock, J., Ruff, S.W., Soderblom, L.A., Squyres, S.W.,  
984 Tosca, N.J., Watters, W.A., Wyatt, M.B., Yen, A., 2005. Provenance and diagenesis  
985 of the evaporite-bearing Burns formation, Meridiani Planum, Mars. *Earth and*  
986 *Planetary Science Letters* 240, 95–121.
- 987 Mège, D., Masson, P., 1996a. Amounts of stretching in Valles Marineris. *Planet. Space*  
988 *Sci.* 44, 749–782.
- 989 Mège, D., Masson, P., 1996b. Stress models for Tharsis formation, Mars. *Planet. Space*  
990 *Sci.* 44, 1471–1497.
- 991 Mège, D., Masson, P., 1996c. A plume tectonics model for the Tharsis province, Mars.  
992 *Planet. Space Sci.* 44, 1499–1546.
- 993 Meresse, S., Costard, F., Mangold, N., Masson, P., Neukum, G., the HRSC Co-I Team,  
994 2008. Formation and evolution of the chaotic terrains by subsidence and  
995 magmatism: Hydraotes Chaos, Mars. *Icarus* 194, 487–500,  
996 doi:10.1016/j.icarus.2007.10.023.

- 997 Michael G., Neukum G., 2007. Refinement of cratering model age for the case of partial  
998 resurfacing. In: Proc. Lunar Planet. Sci. Conf. 38th, #1825.
- 999 Milliken, R.E., Swayze, G.A., Arvidson, R.E., Bishop, J.L., Clark, R.N., Ehlmann, B.L.,  
1000 Green, R.O., Grotzinger, J.P., Morris, R.V., Murchie, S.L., Mustard, J.F., Weitz, C.,  
1001 2008. Opaline silica in young deposits on Mars, *Geology* 36, 847–850.
- 1002 Miyamoto, H., Itoh, K., Komatsu, G., Baker, V.R., Dohm, J.M., Tosaka, H., Sasaki, S.,  
1003 2006. Numerical simulations of large-scale cataclysmic floodwater: A simple  
1004 depth-averaged model and an illustrative application. *Geomorphology* 76, 179–192.
- 1005 Miyamoto, H., Komatsu, G., Baker, V.R., Dohm, J.M., Itoh, K., Tosaka, H., 2007.  
1006 Cataclysmic Scabland flooding: Insights from a simple depth-averaged numerical  
1007 model. *Environmental Modelling and Software* 22, 1400–1408,  
1008 doi:10.1016/j.envsoft.2006.07.006.
- 1009 Montgomery, D.R., Gillespie, A., 2005. Formation of Martian outflow channels by  
1010 catastrophic dewatering of evaporite deposits. *Geology* 33, 625–628.
- 1011 Montgomery, D., Som, S., Schreiber, B.C., Jackson, M., Gillespie, A., Adams, J., 2009.  
1012 Continental-scale salt tectonics on Mars and the origin of Valles Marineris and  
1013 associated outflow channels. *Geological Society of America Bulletin* 121,  
1014 117–133, doi: 10.1130/B26307.1.

- 1015 Mustard, J.F., Poulet, F., Gendrin, A., Bibring, J.-P., Langevin, Y., Gondet, B., Mangold,  
1016 N., Bellucci, G., Altieri, F., 2005. Olivine and pyroxene diversity in the crust of  
1017 Mars. *Science* 307, 1594–1597.
- 1018 O'Connor, J.E., 1993. *Hydrology, Hydraulics, and Geomorphology of the Bonneville*  
1019 *Flood*. Geol. Soc. America Special Paper 274, Boulder, Colorado.
- 1020 O'Connor, J.E., Baker V.R., 1992. Magnitudes and implications of peak discharges from  
1021 Glacial Lake Missoula. *Geological Society of America Bulletin* 104, 267–279.
- 1022 Okubo, C.H., McEwen, A.S., 2007. Fracture controlled paleo-fluid flow in Candor  
1023 Chasma, Mars. *Science* 315, 983–985, doi:10.1126/science.1136855.
- 1024 Okubo, C.H., Schultz, R.A., 2005. Evidence of normal faulting and dike intrusion at  
1025 Valles Marineris from pit crater topography. In: *Proc. Lunar Planet. Sci. Conf.*  
1026 36th, Abstract #1008.
- 1027 Okubo, C.H., Schultz, R.A., Chan, M.A., Komatsu, G., and the HiRISE Team, 2009.  
1028 Deformation band clusters on Mars and implications for subsurface fluid flow.  
1029 *Geological Society of America Bulletin*, doi: 10.1130/B26421.1, in press.
- 1030 Ori, G.G., Marinangeli, L., Baliva, A., 2000. Terraces and Gilbert-type deltas in crater  
1031 lakes in Ismenius Lacus and Memnonia (Mars). *J. Geophys. Res.* 105,  
1032 17629–17641.

- 1033 Ormö, J., Komatsu, G., Chan, M.A., Beitle, B., Parry, W.T., 2004. Geological features  
1034 indicative of processes related to the hematite formation in Meridiani Planum and  
1035 Aram Chaos, Mars: A comparison with diagenetic hematite deposits in southern  
1036 Utah, USA. *Icarus* 171, 295–316, doi:10.1016/j.icarus.2004.06.001.
- 1037 Pondrelli, M., Baliva, A., Di Lorenzo, S., Marinangeli, L., Rossi, A.P., 2005. Complex  
1038 evolution of paleolacustrine systems on Mars: An example from the Holden crater.  
1039 *J. Geophys. Res.* 110, E04016, doi:10.1029/2004JE002335.
- 1040 Poulet, F., Gomez, C., Bibring, J.-P., Langevin, Y., Gondet, B., Belluci, G., Mustard, J.F.,  
1041 2007. Martian surface mineralogy from Observatoire pour la Minéralogie, l'Eau,  
1042 les Glaces et l'Activité on board the Mars Express spacecraft (OMEGA/MEx):  
1043 Global mineral maps. *J. Geophys. Res.* 112, E08S02, doi:10.1029/2006JE002840.
- 1044 Quantin, C., Allemand, P., Mangold, N., Dromart, G., Delacourt, C., 2005. Fluvial and  
1045 lacustrine activity on layered deposits in Melas Chasma, Valles Marineris, Mars. *J.*  
1046 *Geophys. Res.* 110, E12S19, doi:10.1029/2005JE002440.
- 1047 Quantin, C., A. Gendrin, N. Mangold, J.-P. Bibring, E. Hauber, P. Allemand, Omega  
1048 Team, 2006. Stratigraphy and elevation distribution of sulfate deposits in Valles  
1049 Marineris. In: *Proc. Lunar Planet. Sci. Conf.* 37th, Abstract #2046.
- 1050 Robinson, M.S., Tanaka, K.L., 1990. Magnitude of a catastrophic flood event at Kasei

- 1051 Valles, Mars. *Geology* 18, 902–905.
- 1052 Rodriguez, J.A.P., Sasaki, S., Miyamoto, H., 2003. Nature and hydrological relevance of  
1053 the Shalbatana complex underground cavernous system. *Geophys. Res. Lett.* 30(6),  
1054 1304, doi:10.1029/2002GL016547.
- 1055 Rodriguez, J.A.P., Sasaki, S., Dohm, J.M., Tanaka, K.L., Strom, B., Kargel, J., Kuzmin,  
1056 R., Miyamoto, H., Spray, J.G., Fairén, A.G., Komatsu, G., Kurita, K., Baker, V.,  
1057 2005a. Control of impact crater fracture systems on subsurface hydrology, ground  
1058 subsidence and collapse, Mars. *J. Geophys. Res.* 110, E06003,  
1059 doi:10.1029/2004JE002365.
- 1060 Rodriguez, J.A.P., Sasaki, S., Kuzmin, R.O., Dohm, J.M., Tanaka, K.L., Miyamoto, H.,  
1061 Kurita, K., Komatsu, G., Fairén, A.G., Ferris, J.C., 2005b. Outflow channel sources,  
1062 reactivation and chaos formation, Xanthe Terra, Mars. *Icarus* 175, 36–57.
- 1063 Rodriguez, J.A.P., Kargel, J., Crown, D.A., Bleamaster III, L.F., Tanaka, K.L., Baker, V.,  
1064 Miyamoto, H., Dohm, J.M., Sasaki, S., Komatsu, G., 2006. Headward growth of  
1065 chasmata by volatile outbursts, collapse, and drainage: Evidence from Ganges  
1066 chaos, Mars. *Geophys. Res. Lett.* 33, L18203, doi:10.1029/2006GL026275.
- 1067 Rodriguez, J.A.P., Tanaka, K.L., Kargel, J.S., Dohm, J.M., Kuzmin, R., Fairén, A.G.,  
1068 Sasaki, S., Komatsu, G., Schulze-Makuch, D., Jianguo, Y., 2007. Formation and

- 1069 disruption of aquifers in southwestern Chryse Planitia, Mars. *Icarus* 191, 545–567,  
1070 doi:10.1016/j.icarus.2007.05.021.
- 1071 Rossi, A. P., Neukum, G., Pondrelli, M., van Gasselt, S., Zegers, T., Hauber, E., Chicarro,  
1072 A., Foing, B., 2008. Large-scale spring deposits on Mars? *J. Geophys. Res.* 113,  
1073 E08016, doi:10.1029/2007JE003062.
- 1074 Rotto, S., Tanaka K.L., 1995. Geologic/geomorphologic map of the Chryse Planitia  
1075 region of Mars, scale 1:5,000,000. U.S. Geol. Surv. Misc. Invest. Ser., Map  
1076 I-2441.
- 1077 Russell, P.S., Head J.W., III, 2007. The Martian hydrologic system: Multiple recharge  
1078 centers at large volcanic provinces and the contribution of snowmelt to outflow  
1079 channel activity. *Planet. Space Sci.* 55, 315–332, doi:10.1016/j.pss.2006.03.010.
- 1080 Schultz, R.A., 1989. Do pit crater chains grow up to be Valles Marineris canyons? In  
1081 Proceedings of MEVTV Workshop on Tectonic Features on Mars (T. R. Watters  
1082 and M. P. Golombek, Eds.), pp. 47–48 (abstract). LPI Technical Report 89–06.
- 1083 Schultz, R.A., 1998. Multiple-process origin of Valles Marineris and troughs, Mars.  
1084 *Planet. Space Sci.* 46, 827–834.
- 1085 Scott, D.H., Tanaka, K.L., 1986. Geologic map of the western equatorial region of Mars.  
1086 U. S. Geological Survey Miscellaneous Investigation Map I-1802-A.

- 1087 Seidelmann, P.K., Abalakin, V.K., Bursa, M., Davies, M.E., De Bergh, C., Lieske, J.H.,  
1088 Oberst, J., Simon, J.L., Standish, E.M., Stooke, P., Thomas, P.C., 2002. Report of  
1089 the IAU/IAG Working Group on cartographic coordinates and rotational elements  
1090 of the planets, and satellites: 2000. *Celest. Mech. Dyn. Astron.* 82, 83–110.
- 1091 Smith, D., Neumann, G., Ford, P., Guinness, E.A., Slavney, S., 1999. Mars Global  
1092 Surveyor Laser Altimeter Precision Experiment Data Record, NASA Planetary  
1093 Data System, MGS-M-MOLA-3-PEDR-L1A-V1.0, vols.  
1094 MGSL\_0001-MGSL\_0054.
- 1095 Tanaka, K.L., Scott, D.H., Greeley, R., 1992. Global stratigraphy. In: Mars (Kieffer,  
1096 H.H., et al., eds.), University of Arizona Press, Tucson, 345–382.
- 1097 Treiman, A.H., 2008. Ancient groundwater flow in the Valles Marineris on Mars  
1098 inferred from fault trace ridges. *Nature Geoscience* 1, 181–183,  
1099 doi:10.1038/ngeo131.
- 1100 Wessel, P., Smith, W.H.F., 1998. New, improved version of Generic Mapping Tools  
1101 released. *EOS trans, AGU*, 79, 579.
- 1102 Williams, R.M., Phillips, R.J., Malin, M.C., 2000. Flow rates and duration within Kasei  
1103 Valles, Mars: Implications for the formation of a Martian ocean. *Geophys. Res.*  
1104 *Lett.* 27, 1073–1076.

- 1105 Wilson, L., Ghatan, G.J., Head III, J.W., Mitchell K. L., 2004. Mars outflow channels: A  
1106 reappraisal of the estimation of water flow velocities from water depths, regional  
1107 slopes, and channel floor properties. *J. Geophys. Res.* 109, E09003,  
1108 doi:10.1029/2004JE002281.
- 1109 Wise, D.U., Golombek, M.P., McGill, G.E., 1979. Tharsis province of Mars: geologic  
1110 sequence, geometry and a deformation mechanism. *Icarus* 38, 456–72.
- 1111 Wyrick, D., Ferrill, D.A., Morris, A.P., Colton, S.L., Sims, D.W., 2004. Distribution,  
1112 morphology, and origins of Martian pit crater chains. *J. Geophys. Res.* 109,  
1113 E06005, doi:10.1029/2004JE002240.

1114 **Figure captions**

1115

1116 **Fig. 1.** Location map (MOLA topography) of the Valles Marineris-chaotic terrain  
1117 transition zone and the study area. The rectangle shows the area of **Fig. 2.**

1118

1119 **Fig. 2.** THEMIS infrared daytime image mosaic of the study area, Aurorae and Ophir  
1120 plana.

1121

1122 **Fig. 3.** Cumulative crater population plot of the plains unit around Ganges Chasma.  
1123 The plot was made using the Craterstats software (Michael and Neukun, 2007).

1124

1125 **Fig. 4.** 3-dimensional view of Elaver Vallis in Aurorae Planum south of Ganges  
1126 Chasma (THEMIS infrared daytime image mosaic draped on MOLA topography; inset  
1127 from THEMIS visible image V10051003). Elaver Vallis is characterized by the  
1128 morphology of an outflow channel system. The primary source for the flooding is the  
1129 Morella basin (70-80 km in diameter), but fluid could have originated also from the  
1130 patches of chaotic terrain observed in the middle reach. Elaver Vallis terminates on the  
1131 floor of Ganges Chasma. The large Elaver fan complex is placed in front of the Elaver  
1132 Vallis mouth and smaller fans exist to both sides of this complex. These fans are  
1133 coalesced (bajadas). The arrow in the inset (a) indicates an erosional margin of the  
1134 Elaver fan complex cutting an adjacent smaller fan.

1135

1136 **Fig. 5.** a) Overview of the Elaver Vallis region from THEMIS infrared daytime image  
1137 mosaic. Locations of images in **Fig. 6** and topographic profiles in **Fig. 7** are also  
1138 shown. b) MOLA topography of the Elaver Vallis region.

1139

1140 **Fig. 6.** Detailed characteristics of Elaver Vallis. a) Near terminal reach of Elaver  
1141 Vallis. A cross-cutting relationship is observable between two grooved reaches  
1142 (THEMIS visible image V10051003). b) Grooves exist on a portion of plains  
1143 separated from Elaver Vallis (THEMIS visible image V15255002). c) Patches of  
1144 chaotic terrain are distributed in the middle reach of Elaver Vallis (THEMIS visible  
1145 image V10076002).

1146

1147 **Fig. 7.** A topographic profile (A-A') across the Morella basin stretches down to the  
1148 floor of Ganges Chasma. Longitudinal (B-B') and cross-sectional (b-b') profiles of  
1149 Elaver Vallis. Longitudinal (C-C') and cross-sectional (c-c') profiles of the lowermost

1150 part of Elaver Vallis. See **Fig. 5a** for their locations. These profiles were derived  
1151 from the MOLA gridded data set.

1152

1153 **Fig. 8.** The Morella basin and Ganges Cavus (HRSC nadir image from orbit 0394\_2).  
1154 The Morella basin is connected with Elaver Vallis with a spillway to the east. A crater  
1155 named Johnstown with irregular rim is observed on the basin floor (J). Locations of  
1156 images in **Fig. 9** are shown.

1157

1158 **Fig. 9.** Detailed characteristics of the Morella basin. a) Grooves near the spillway  
1159 (THEMIS visible image V08179002). b) Locally, dark-toned materials exhibit their  
1160 margins raised above the adjacent basin floor (HiRISE red CCD mosaic from orbit  
1161 PSP\_003183\_1705). c) Dark-toned materials observed in channels (MOC narrow  
1162 angle image R0501760). d) A channel originating from a shallow depression outside  
1163 of the Morella basin (THEMIS visible image V11661002).

1164

1165 **Fig. 10.** THEMIS infrared images of the Morella basin: a) THEMIS daytime image  
1166 mosaic b) THEMIS nighttime image mosaic. The horizontal strips are artifacts.

1167

1168 **Fig. 11.** a) Three elevations corresponding to possible paleolake levels within the  
1169 Morella basin (MOLA contours over HRSC nadir image from orbit 0394\_2). b)  
1170 Pyroxene distribution determined by OMEGA observation (orbit 0394\_2). Olivine  
1171 mineral distributions determined by OMEGA observation (orbit 0394\_2): c) forsterite;  
1172 d) fayalite. White bars indicate the eastern limit of the OMEGA orbit coverage. The  
1173 lower numbers on the scale bars are the minimum value or the detection threshold (see  
1174 Poulet et al., 2007) of spectral parameters that represent the absorption band depth for  
1175 each mineral.

1176

1177 **Fig. 12.** Ophir Planum west of the Morella basin (THEMIS infrared daytime image  
1178 mosaic). Allegheny Vallis originates from an elongated depression called Ophir Cavus.  
1179 Topographic profiles of its lower reach are shown below. Walla Walla Vallis originates  
1180 from a pit-crater chain. A probable deltaic body was formed in front of a valley in the  
1181 rim of a 40-km-diameter basin. Locations of **Figs. 13, 14, 15** are shown.

1182

1183 **Fig. 13.** Details of sources of Allegheny Vallis. a) This image shows a terraced upper  
1184 reach of Allegheny Vallis near Ophir Cavus (HiRISE red CCD mosaic from orbit  
1185 PSP\_005082\_1700). b) Layered outcrops occur on the bottom of Ophir Cavus.

1186 (HiRISE red CCD mosaic from orbit PSP\_005082\_1700). c) A branch of Allegheny  
1187 Vallis originates from shallow depressions (THEMIS infrared daytime image).

1188

1189 **Fig. 14.** Details of the area where Walla Walla Vallis originates from a pit-crater chain  
1190 (THEMIS visible image V10176001).

1191

1192 **Fig. 15.** a) A 40-km-diameter basin east of the Wallula basin hosts a variety of  
1193 features indicative of paleo-hydrological processes. A possible fan delta is positioned  
1194 in front of a valley in the rim. Its delta front elevation (~1300 m) coincides with  
1195 terminations of channels inward of the rim (HRSC nadir image from orbit 100). A  
1196 small valley is incised into a massif east of the basin (V). b) Details of the possible fan  
1197 delta. Layers are observed in the steep front slopes (L) (HiRISE red CCD mosaic from  
1198 orbit PSP\_005583\_1700 and MOC narrow angle image S1600444).

1199

1200 **Fig. 16.** a) Regional MOLA topography of Aurorae and Ophir plana. Ophir and  
1201 Ganges cavi are in line with depression features including Ophir Catenae and large  
1202 canyons of Candor Chasma, implying a genetic connection of these features. b) It is  
1203 hypothesized that the fluid emerging at least partially through Ganges Cavus or its  
1204 incipient depression filled the Morella basin and spilled out of the basin to the east,  
1205 forming Elaver Vallis. Fluid emerged from Ophir Cavus formed Allegheny Vallis. A  
1206 local elevation level of 2250 m is shown. The Wallula basin may have received fluid  
1207 from a pit-crater chain to its south. A 40-km-diameter basin appears to have hosted a  
1208 paleolake.

Table 1. Estimated volumes of the purported paleolake in the Morella basin.

Shoreline level (m)*	Inferred from	Volume (km <sup>3</sup> )
1780	Cross-over channel	2773
1250	Spillway	377
1200	Terminations of channels	199
1120	Terminations of channels	42
Ganges Cavus		2202

\*Based on the gridded PEDR. The volume estimations for 1120, 1200, 1250 and 1780 m do not include the volume of Ganges Cavus.

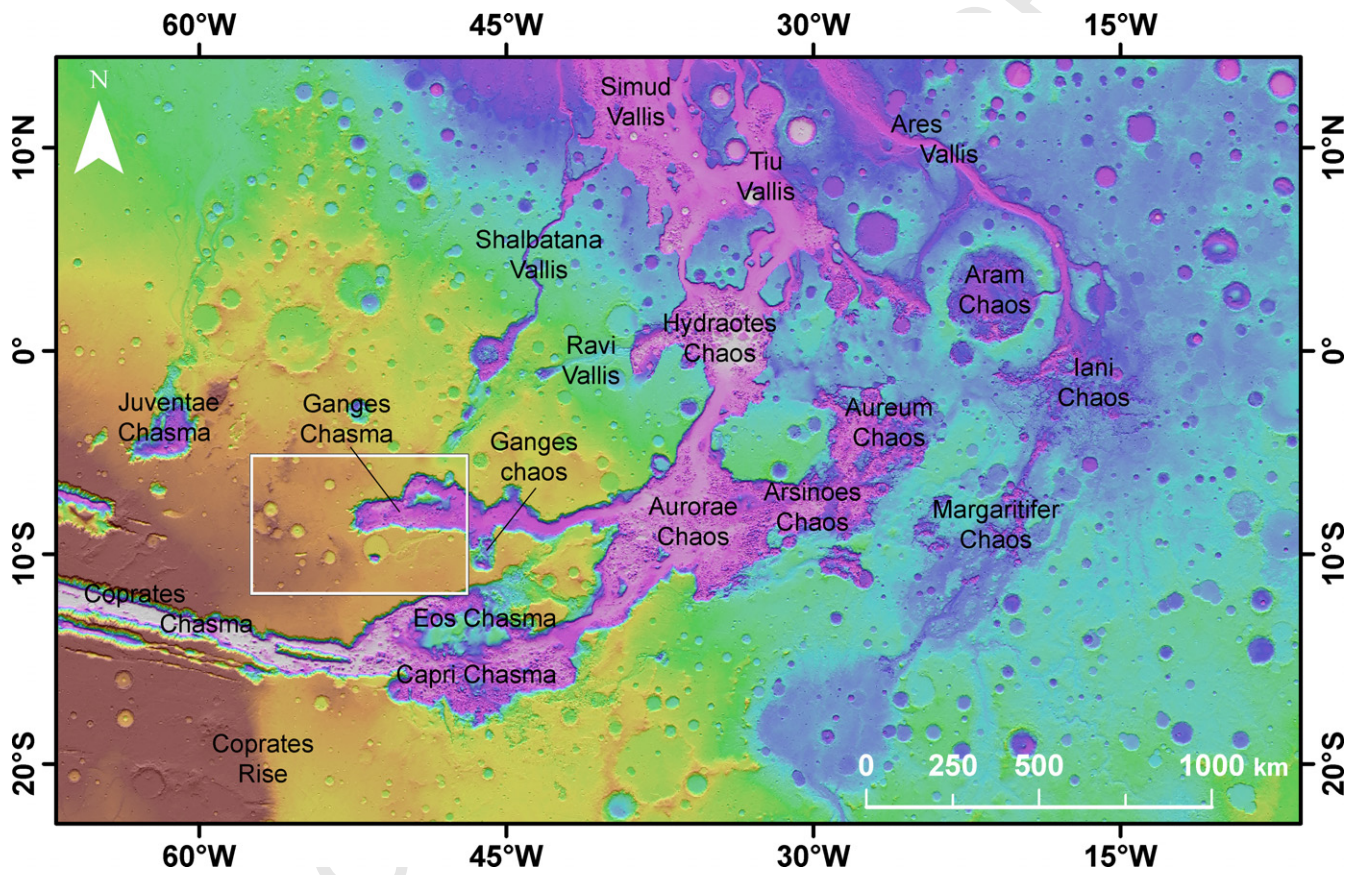


fig1\_color

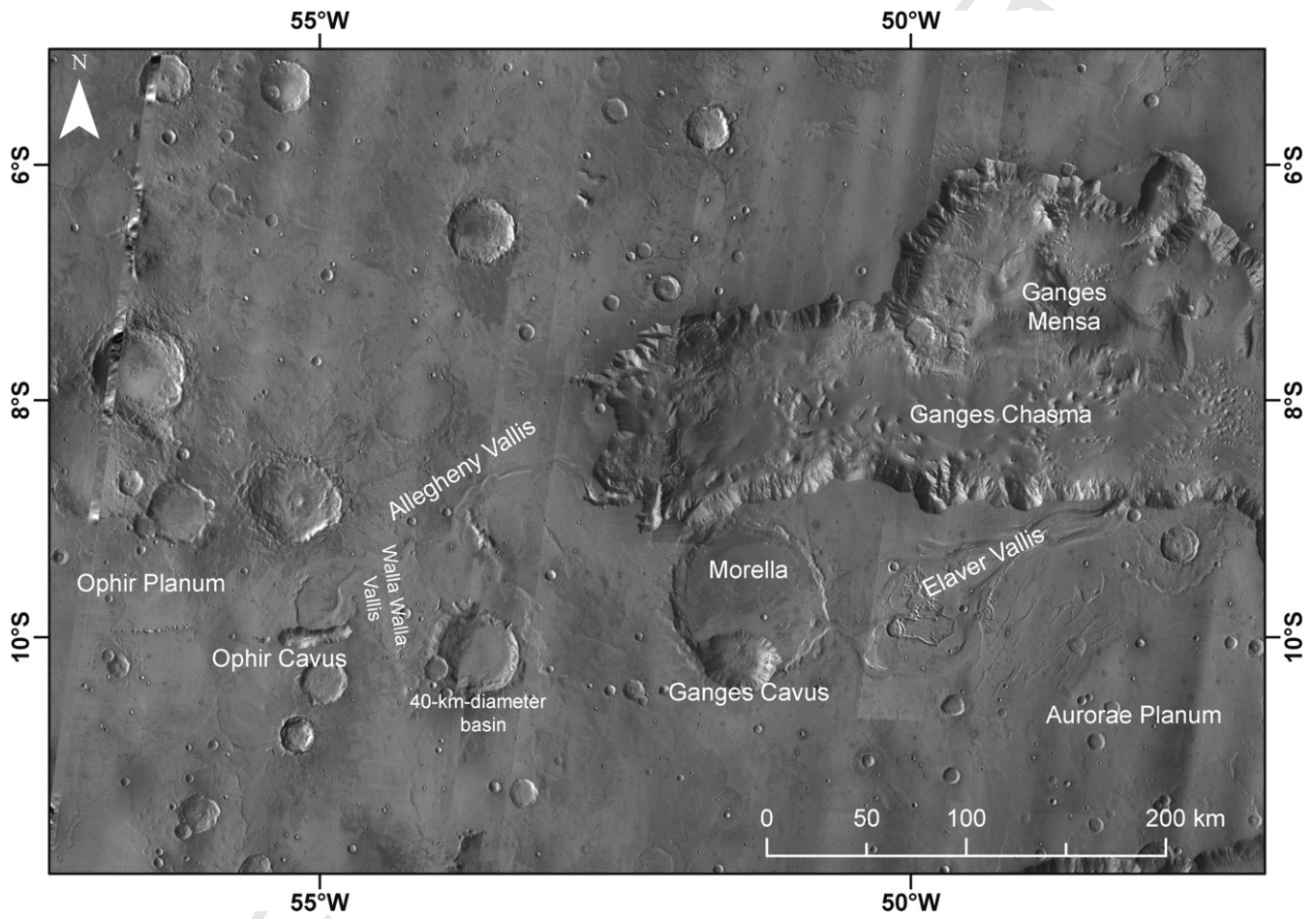
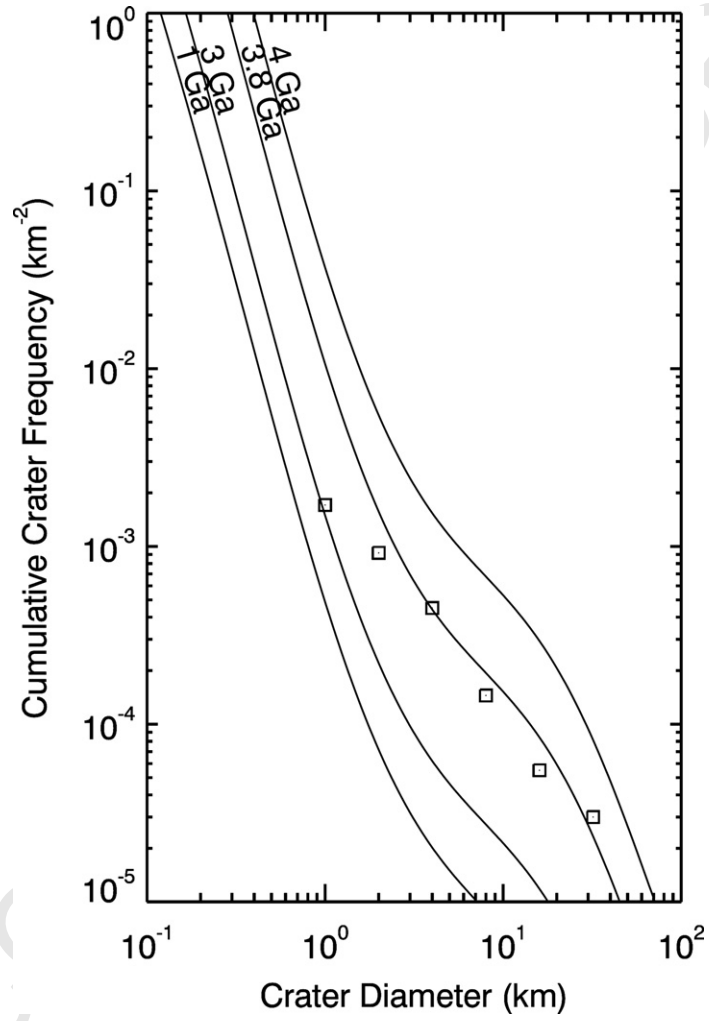


fig2



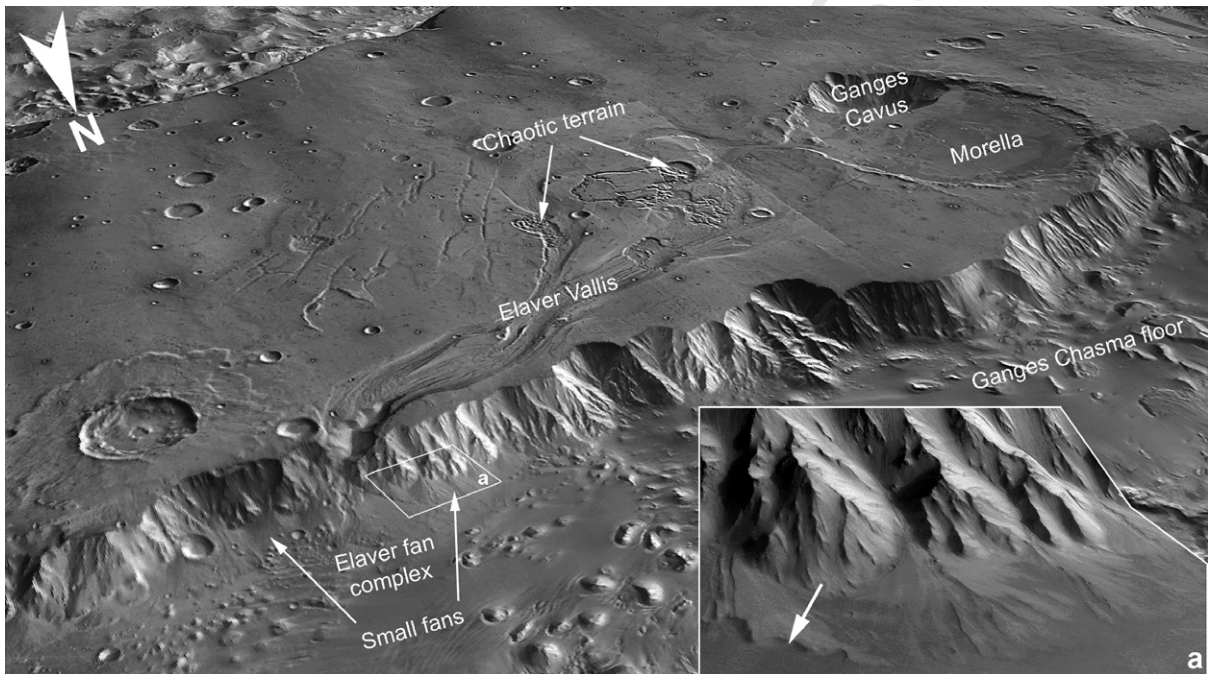


fig4

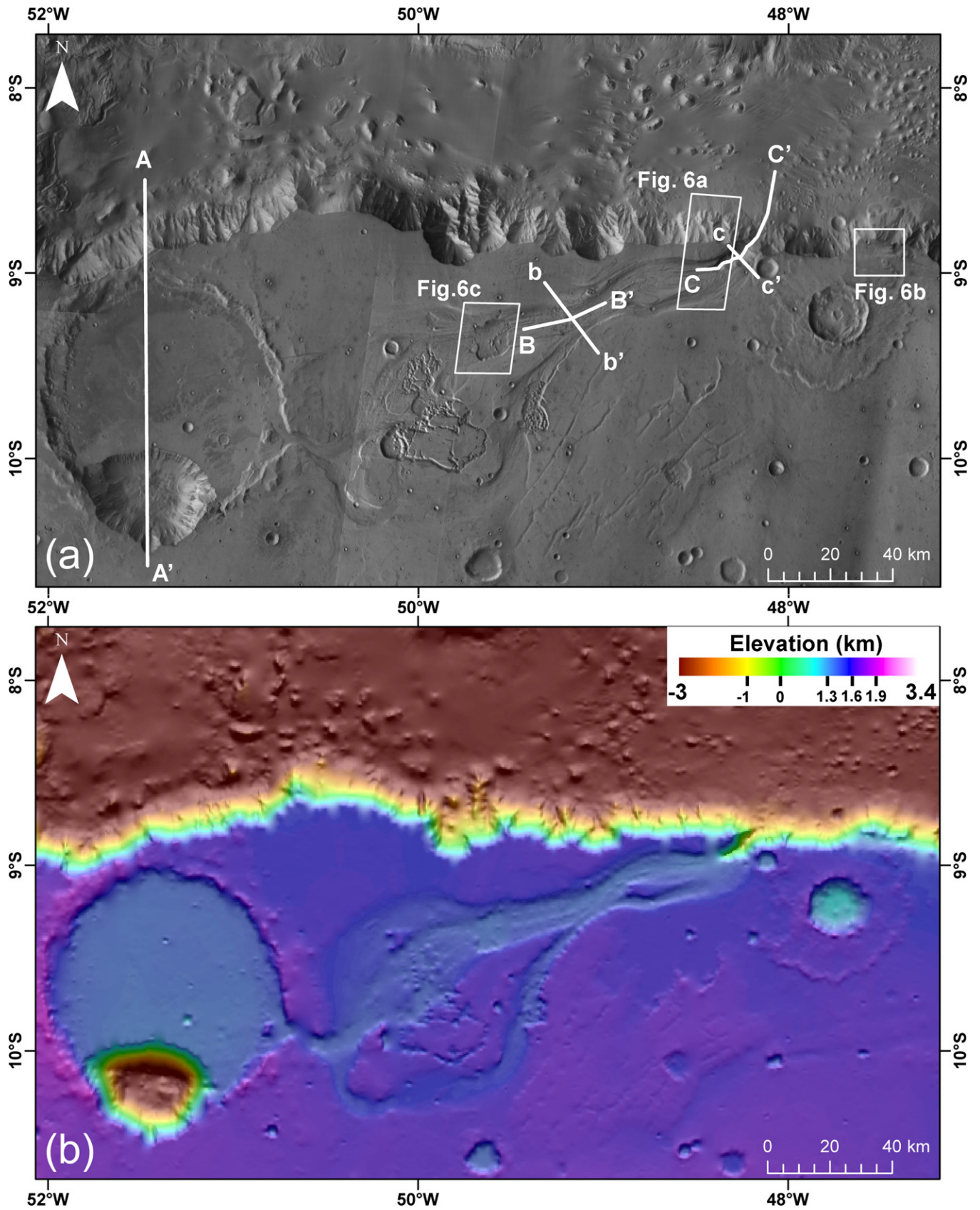


fig5\_color

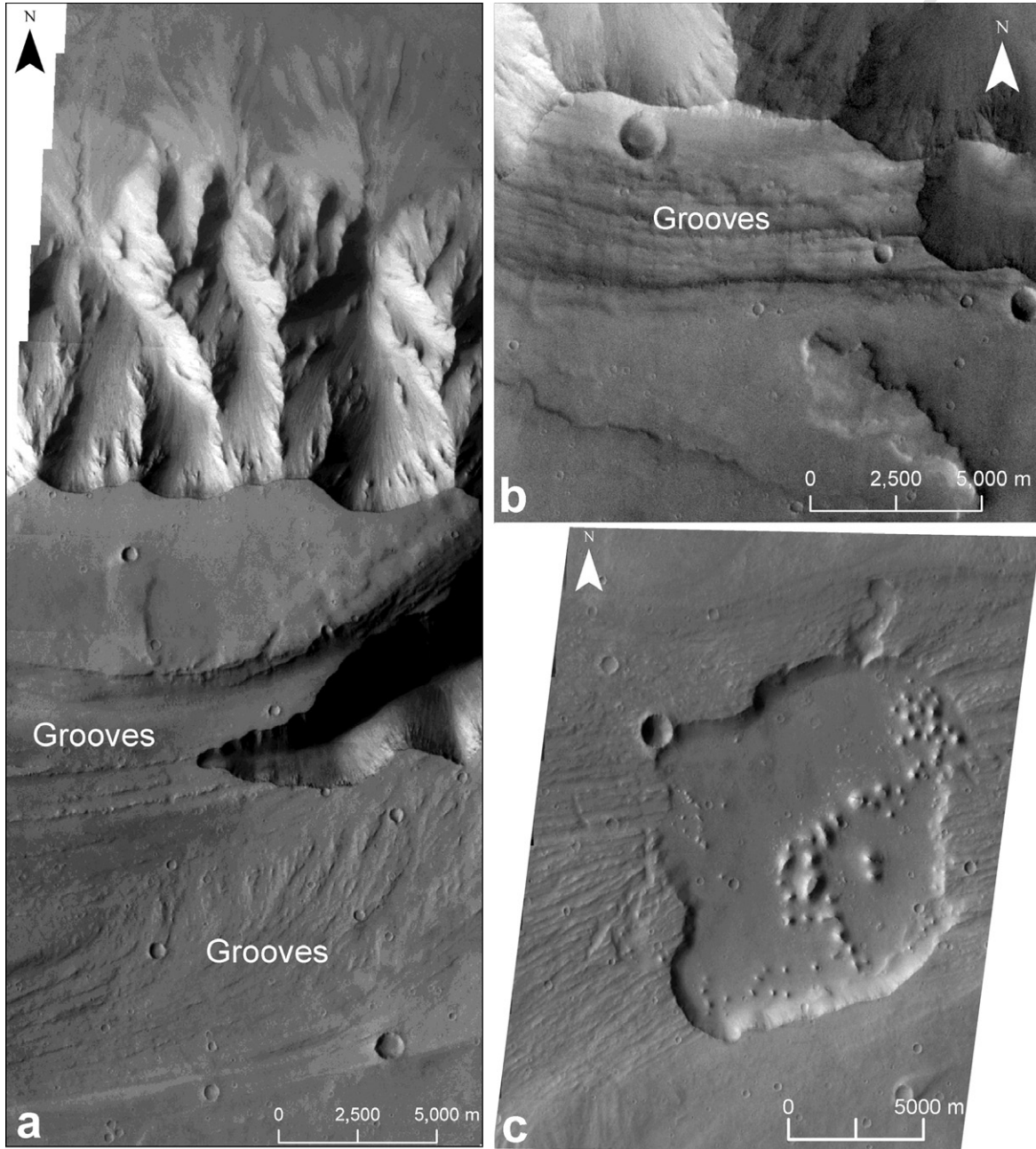


fig6

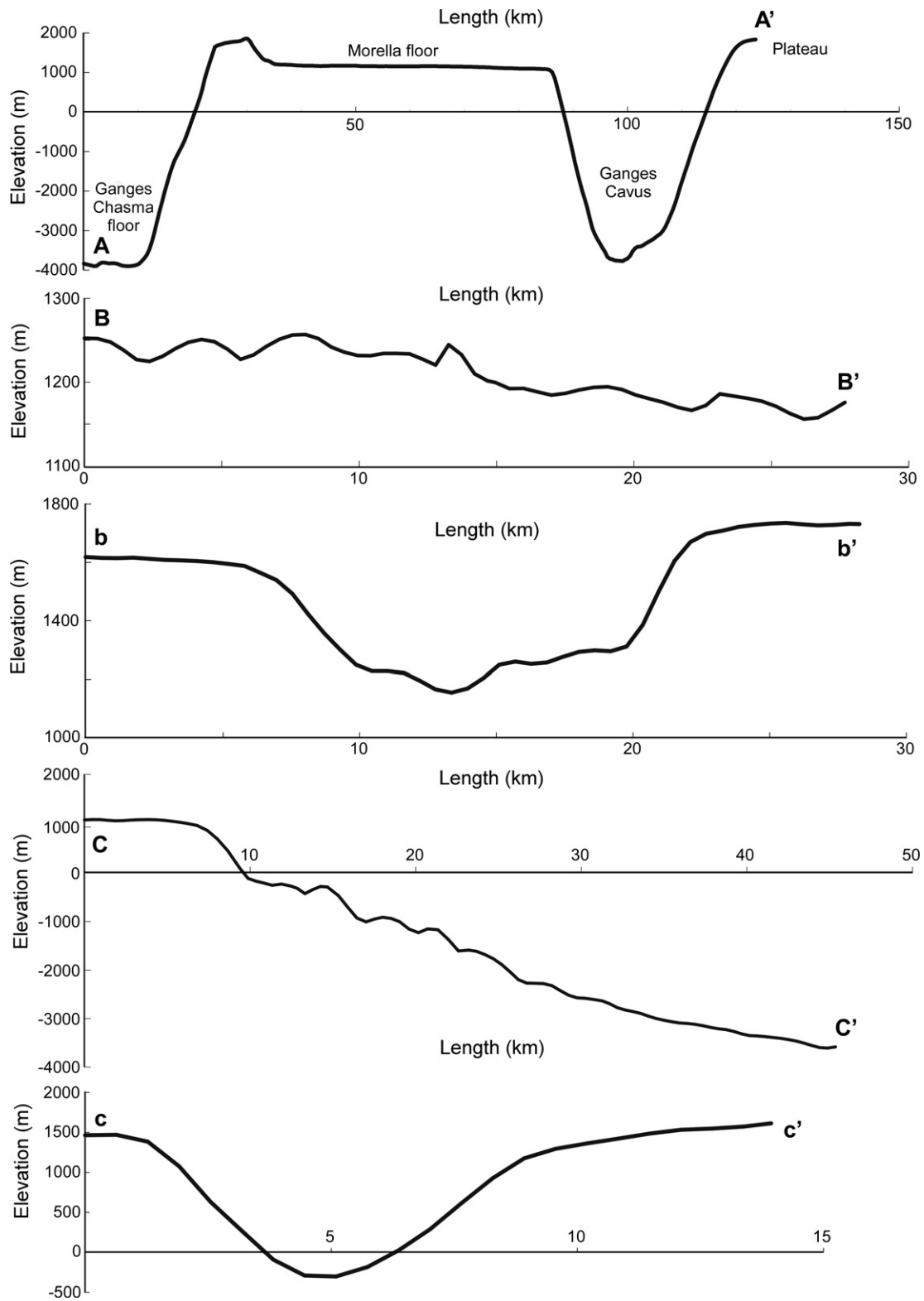
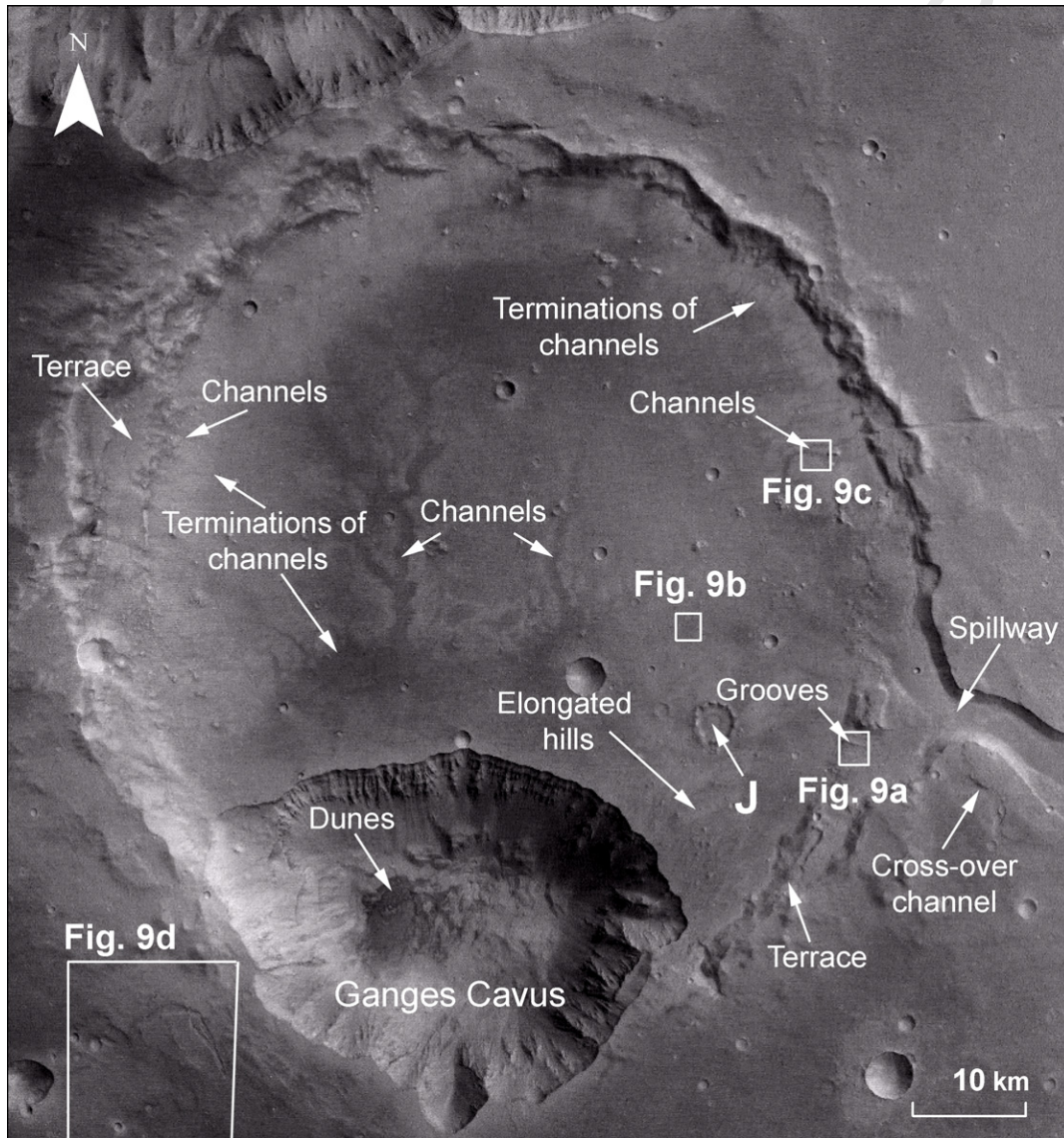


Fig7



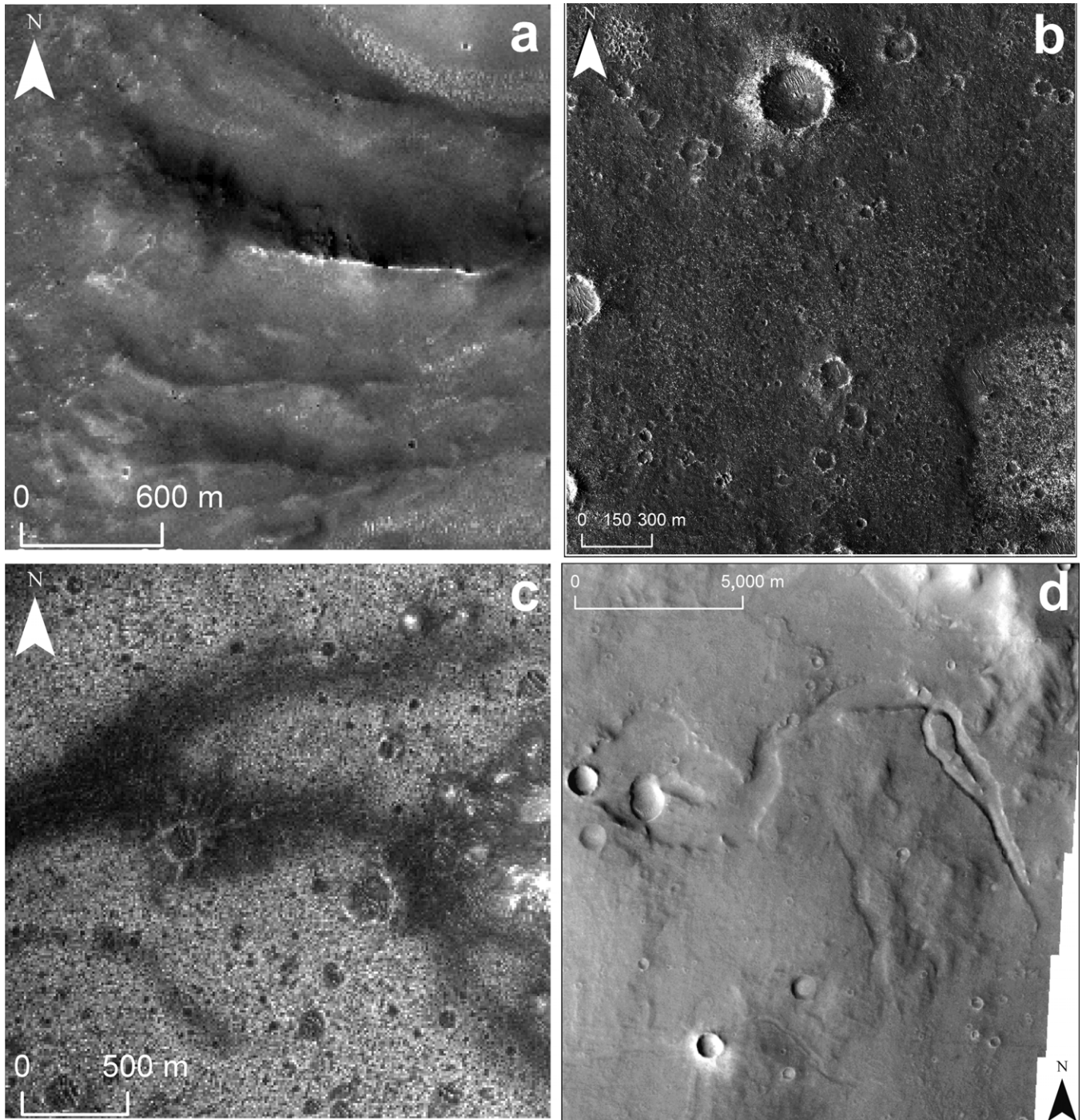


fig9

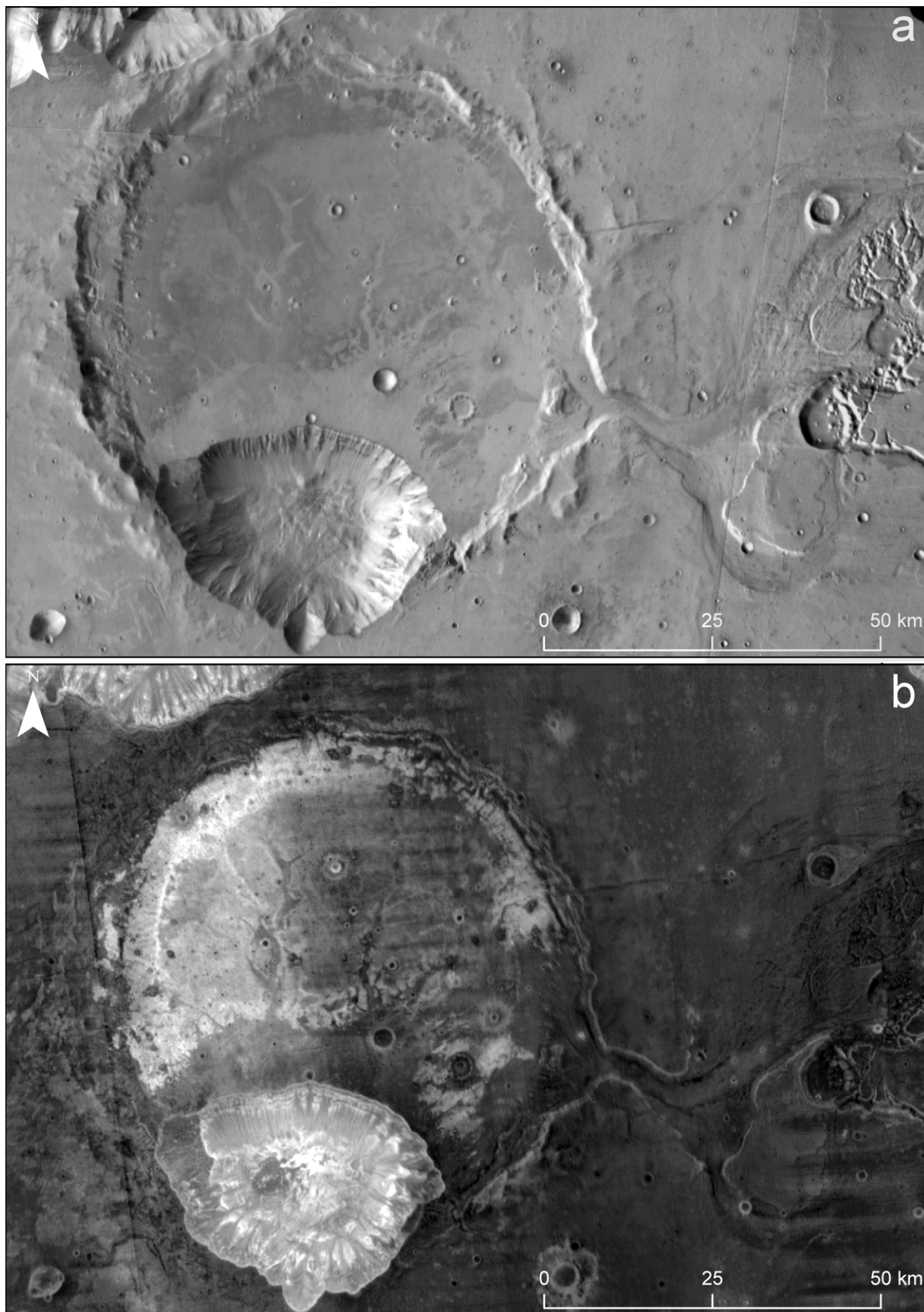


fig10

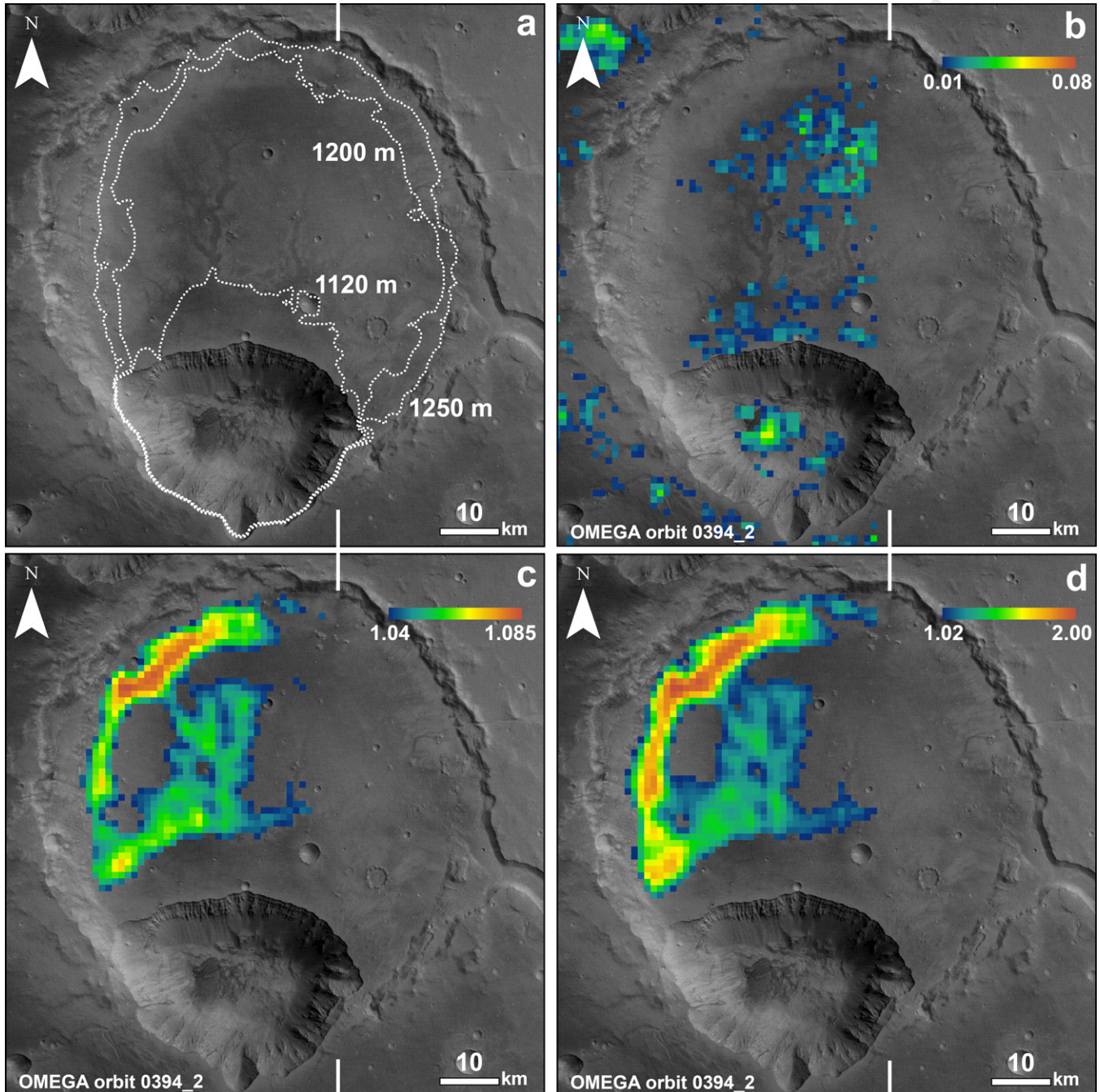


fig11\_color

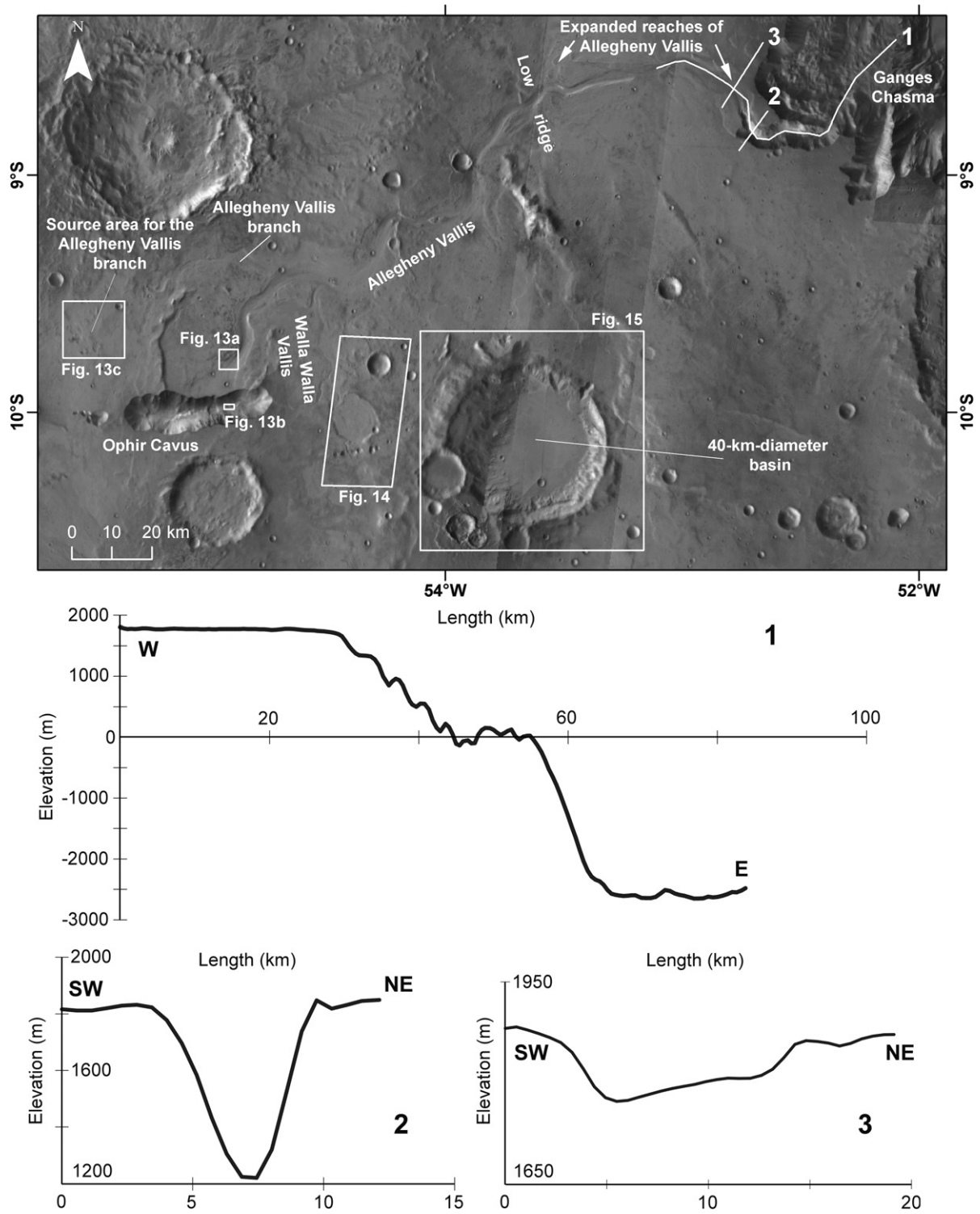


fig12

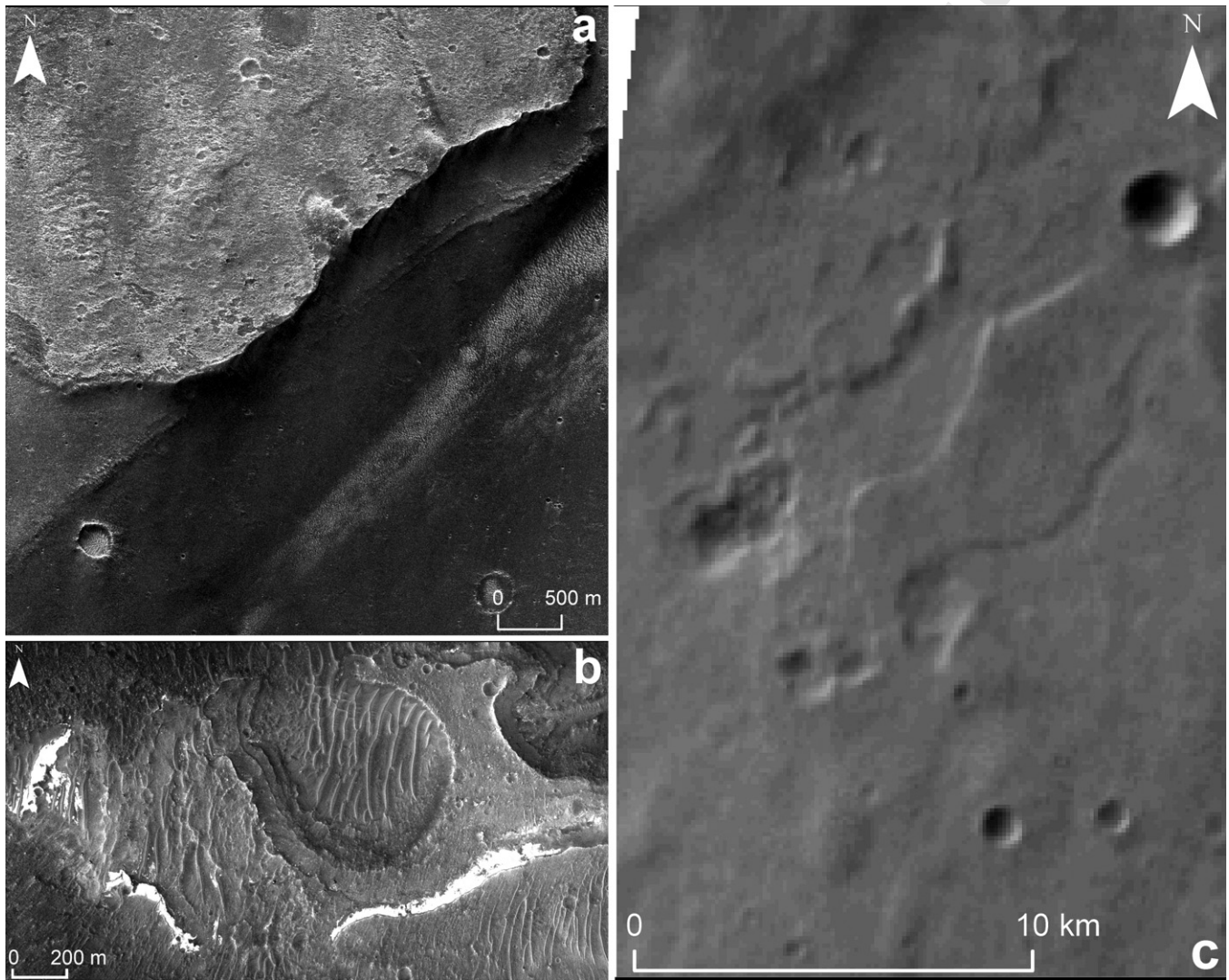


fig13

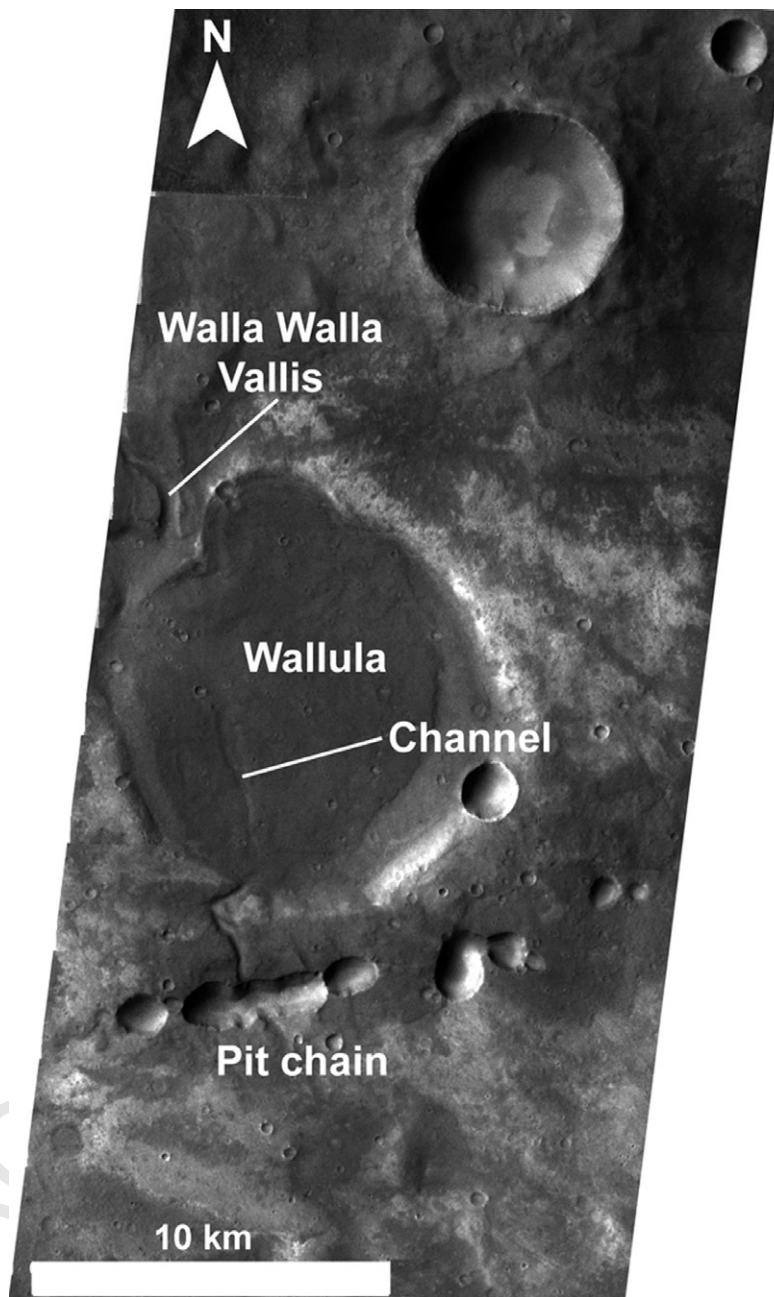


FIG14

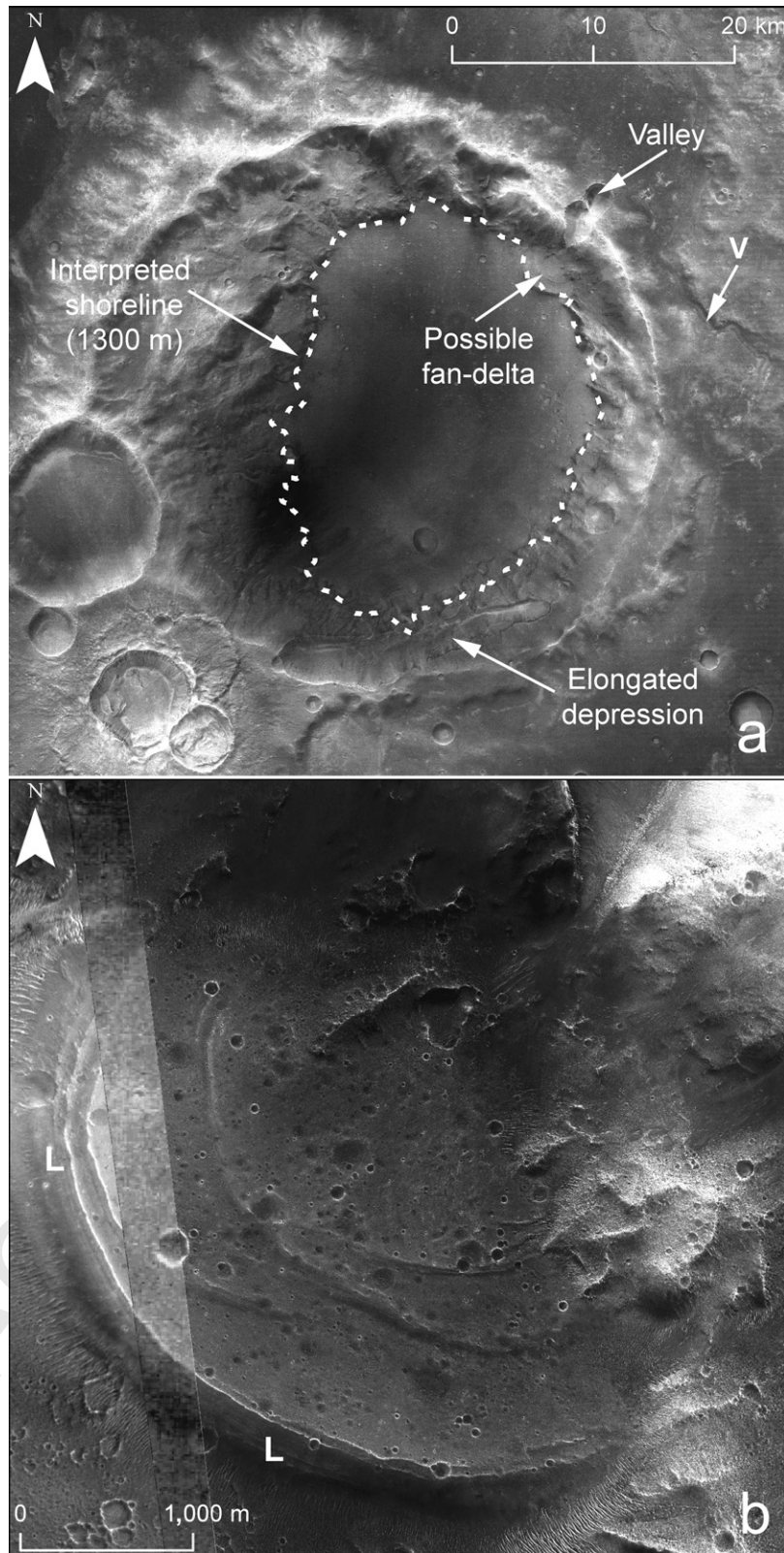


fig15

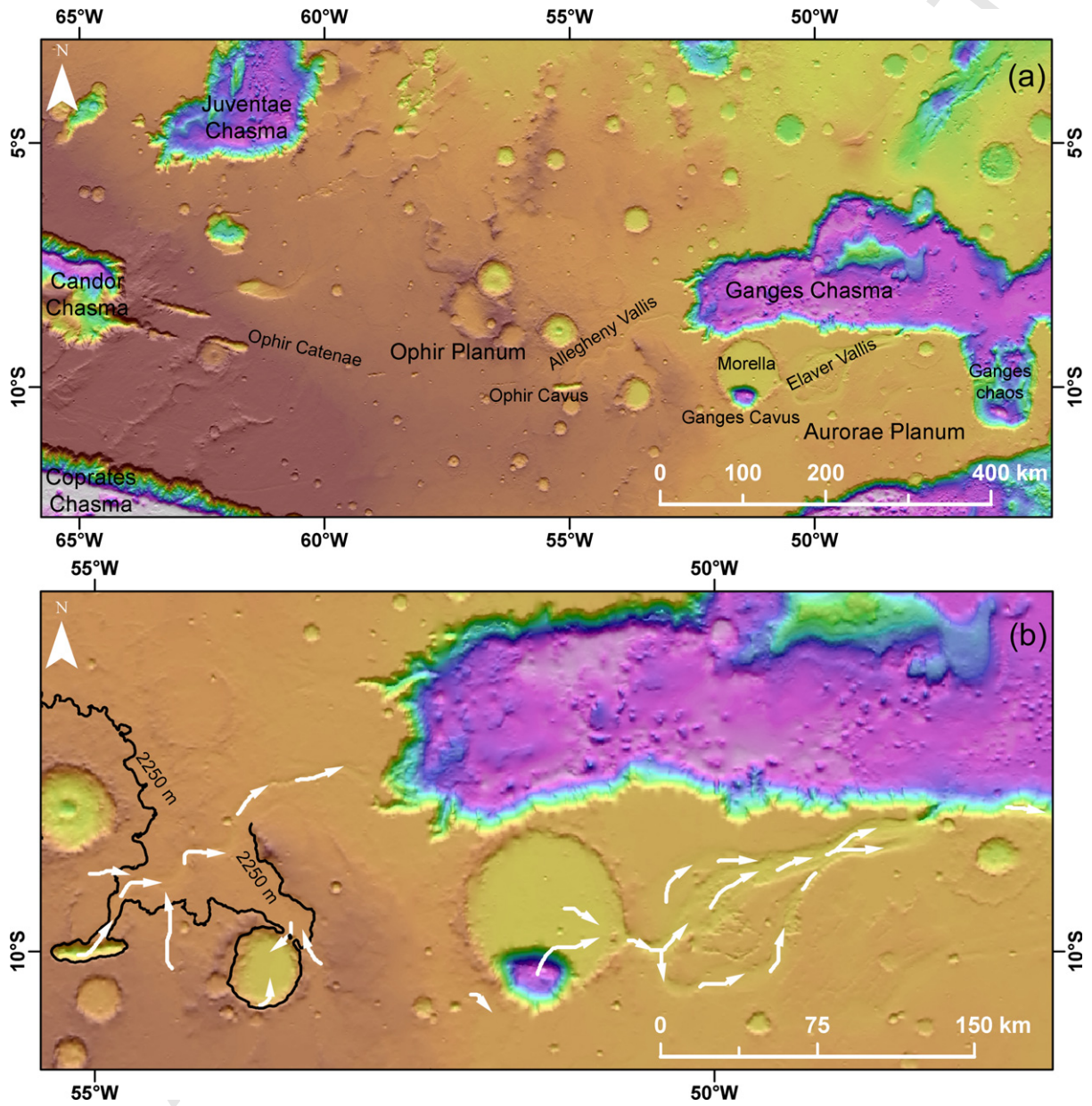


fig16\_color